

CR 193974

SwRI Project 15-4865
30 April 1994

NAS8-32489

A Final Report for

**Participation in the Definition, Conduct, and Analysis of Particle
Accelerator Experiments for the First Spacelab Mission**

Prepared for:

**George C. Marshall Space Flight Center
Marshall Space Flight Center, Alabama 35812**

Prepared by:

J. L. Burch

(NASA-CR-193974) PARTICIPATION IN
THE DEFINITION, CONDUCT, AND
ANALYSIS OF PARTICLE ACCELERATOR
EXPERIMENTS FOR THE FIRST SPACELAB
MISSION Final Report (Southwest
Research Inst.) 56 p

N94-35483

Unclass

G3/73 0013757



SOUTHWEST RESEARCH INSTITUTE
Instrumentation and Space Research Division
6220 Culebra Road, San Antonio, Texas 78238-5166
(210) 684-5111 • FAX (210) 647-4325

PARTICIPATION IN THE DEFINITION, CONDUCT, AND ANALYSIS
OF PARTICLE ACCELERATOR EXPERIMENTS
FOR THE FIRST SPACELAB MISSION

30 April 1994

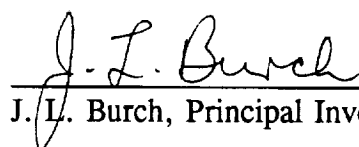
Final Report
Contract No. NAS8-32488
SwRI Project 15-4865

by

J. L. Burch

for

George C. Marshall Space Flight Center
Marshall Space Flight Center, Alabama 35812



J. L. Burch, Principal Investigator

1. The first part of the document is a list of the names of the persons who have been named in the proceedings.

2. The second part of the document is a list of the names of the persons who have been named in the proceedings.

3. The third part of the document is a list of the names of the persons who have been named in the proceedings.

4. The fourth part of the document is a list of the names of the persons who have been named in the proceedings.

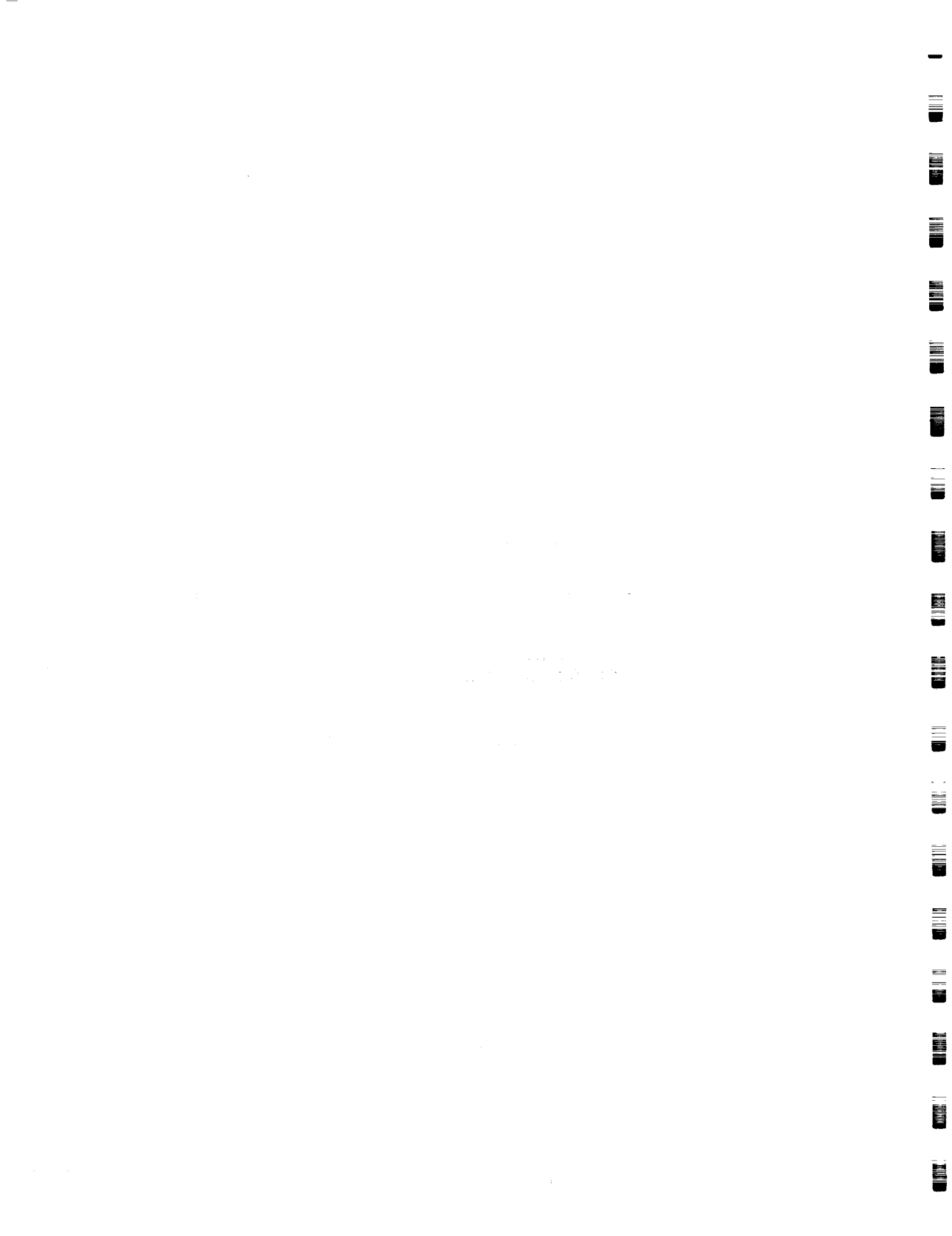
5. The fifth part of the document is a list of the names of the persons who have been named in the proceedings.

DISTRIBUTION LIST

This report addressed to the National Aeronautics and Space Administration, George C. Marshall Space Flight Center, Marshall Space Flight Center, Alabama, 35812, has been distributed as follows:

Code	No. Copies
AP 32	1
JA53/Dinah Higgins	2
CN22D	3
NASA Lewis Res. Center MS 302-1/C. K. Purvis 21000 Brookpark Road Cleveland, OH 44135	2
NASA Scientific & Technical Information Facility	2

****Copy of letter of transmittal plus copy of Technical Report.**



I. INTRODUCTION

The Space Experiments with Particle Accelerators (SEPAC) is a joint endeavor between NASA and the Institute of Space and Aeronautical Sciences (ISAS) in Japan. Its objectives are to use energetic electron beams to investigate beam-atmosphere interactions and beam-plasma interactions in the Earth's upper atmosphere and ionosphere using the Shuttle Spacelab. Two flights of SEPAC have occurred to date (Spacelab 1 on STS-9 in November-December 1983 and ATLAS 1 on STS-45 in March-April 1992). The SEPAC instrumentation is available for future missions, and the scientific results of the first two missions justify further investigations; however, at present there are no identifiable future flight opportunities. As specified in the contract, the primary purpose of this report is to review the scientific accomplishments of the ATLAS 1 SEPAC experiments, which have been documented in the published literature, with only a brief review of the earlier Spacelab 1 results.

One of the main results of the Spacelab 1 SEPAC experiments was that the ejection of plasma from the magneto-plasma-dynamic (MPD) arcjet was effective in maintaining vehicle charge neutralization during electron beam firings, but only for a brief period of 10 ms or so. Therefore, a xenon plasma contactor, which can provide continuous vehicle charge neutralization, was developed for the ATLAS 1 SEPAC experiments. Because of the successful operation of the plasma contactor on ATLAS 1, it was possible to perform experiments on beam-plasma interactions and beam-atmosphere interactions at the highest beam power levels of SEPAC. In addition, the ability of the plasma contactor to eject neutral xenon led to a successful experiment on the critical ionization velocity (CIV) phenomena on ATLAS 1.

II. SPACELAB 1 RESULTS

The results of the Spacelab 1 SEPAC experiments were reported in numerous refereed publications. A subset of those publications, on which Dr. J. L. Burch of SwRI is an author or co-author, is listed below in chronological order:

Obayashi, T., N. Kawashima, K. Kuriki, M. Nagatomo, K. Ninomiya, S. Sasaki, M. Yanagisawa, I. Kudo, M. Ejiri, W. T. Roberts, C. R. Chappell, D. L. Reasoner, J. L. Burch, W. W. L. Taylor, P. M. Banks, P. R. Williamson, and O. K. Garriott, Space experiments with particle accelerators, *Science*, 225, 195, 1984.

Taylor, W. W. L., T. Obayashi, N. Kawashima, S. Sasaki, M. Yanagisawa, J. L. Burch, D. L. Reasoner and W. T. Roberts, Wave-particle interactions induced by SEPAC on Spacelab 1: Wave observations, *Radio Science*, 20, 486-498, 1985.

Obayashi, T., N. Kawashima, S. Sasaki, M. Yanagisawa, K. Kuriki, M. Nagatomo, K. Ninomiya, W. T. Roberts, W. W. L. Taylor, P. R. Williamson, P. Banks, D. L. Reasoner and J. L. Burch, Initial results of SEPAC scientific achievement, in *Earth-Oriented Applications of Space Technology*, 5, Nos. 1/2, 37-45, Pergamon Press, 1985.

1. The first part of the document is a list of the names of the persons who have been appointed to the various offices of the city.

2. The second part of the document is a list of the names of the persons who have been appointed to the various offices of the city.

3. The third part of the document is a list of the names of the persons who have been appointed to the various offices of the city.

4. The fourth part of the document is a list of the names of the persons who have been appointed to the various offices of the city.

5. The fifth part of the document is a list of the names of the persons who have been appointed to the various offices of the city.

6. The sixth part of the document is a list of the names of the persons who have been appointed to the various offices of the city.

7. The seventh part of the document is a list of the names of the persons who have been appointed to the various offices of the city.

8. The eighth part of the document is a list of the names of the persons who have been appointed to the various offices of the city.

9. The ninth part of the document is a list of the names of the persons who have been appointed to the various offices of the city.

10. The tenth part of the document is a list of the names of the persons who have been appointed to the various offices of the city.

11. The eleventh part of the document is a list of the names of the persons who have been appointed to the various offices of the city.

12. The twelfth part of the document is a list of the names of the persons who have been appointed to the various offices of the city.

13. The thirteenth part of the document is a list of the names of the persons who have been appointed to the various offices of the city.

14. The fourteenth part of the document is a list of the names of the persons who have been appointed to the various offices of the city.

15. The fifteenth part of the document is a list of the names of the persons who have been appointed to the various offices of the city.

- Sasaki, S., N. Kawashima, K. Kuriki, M. Yanagisawa, T. Obayashi, W. T. Roberts, D. L. Reasoner, W. W. L. Taylor, P. R. Williamson, P. M. Banks and J. L. Burch, Ignition of beam plasma discharge in the electron beam experiment in space, *Geophys. Res. Lett.*, **12**, 647-650, 1985.
- Sasaki, S., S. Kubota, N. Kawashima, K. Kuriki, M. Yanagisawa, T. Obayashi, W. T. Roberts, D. L. Reasoner, W. W. L. Taylor, P. R. Williamson, P. M. Banks and J. L. Burch, An enhancement of plasma density by neutral gas injection observed in SEPAC Spacelab 1 experiment, *J. Geomag. Geoelectr.*, **37**, 883-894, 1985.
- Sasaki, S., N. Kawashima, K. Kuriki, M. Yanagisawa, T. Obayashi, W. T. Roberts, D. L. Reasoner, W. W. L. Taylor, P. R. Williamson, P. M. Banks and J. L. Burch, Gas ionization induced by a high speed plasma injection in space, *Geophys. Res. Lett.*, **13**, 434-437, 1986.
- Neubert, T., W. W. L. Taylor, L. R. O. Storey, N. Kawashima, W. T. Roberts, D. L. Reasoner, P. M. Banks, D. A. Gurnett, R. L. Williams and J. L. Burch, Waves generated during electron beam emissions from the space shuttle, *J. Geophys. Res.*, **91**, 11,321-11,330, 1986.
- Burch, J. L., Space plasma physics results from Spacelab 1, *J. Spacecraft and Rockets*, **23**, 331-335, 1986.
- Cai, D., T. Neubert, L. R. O. Storey, P. M. Banks, S. Sasaki, K. Abe and J. L. Burch, ELF oscillations associated with electron beam injections from the space shuttle, *J. Geophys. Res.*, **92**, 12,451-12,457, 1987.
- Sasaki, S., N. Kawashima, K. Kuriki, M. Yanagisawa, T. Obayashi, W. T. Roberts, D. L. Reasoner, P. R. Williamson, P. M. Banks, W. W. L. Taylor, K. Akai and J. L. Burch, Neutralization of beam-emitting spacecraft by plasma injection, *J. Spacecraft and Rockets*, **24**, 227-231, 1987.
- Marshall, J. A., C. S. Lin, J. L. Burch, W. Bernstein and C. Beghin, Spacelab 1 experiments on interactions of an energetic electron beam with neutral gas, *J. Spacecraft and Rockets*, **25**, 361-367, 1988.
- Marshall, J. A., C. S. Lin and J. L. Burch, Further studies of ELF oscillations during electron beam firings on Spacelab 1, *IEEE Trans. on Plasma Science*, **18**, 169-170, 1990.

1. The first part of the document is a list of the names of the persons who have been appointed to the various positions of the Board of Directors of the Corporation.

2. The second part of the document is a list of the names of the persons who have been appointed to the various positions of the Board of Directors of the Corporation.

3. The third part of the document is a list of the names of the persons who have been appointed to the various positions of the Board of Directors of the Corporation.

4. The fourth part of the document is a list of the names of the persons who have been appointed to the various positions of the Board of Directors of the Corporation.

5. The fifth part of the document is a list of the names of the persons who have been appointed to the various positions of the Board of Directors of the Corporation.

6. The sixth part of the document is a list of the names of the persons who have been appointed to the various positions of the Board of Directors of the Corporation.

7. The seventh part of the document is a list of the names of the persons who have been appointed to the various positions of the Board of Directors of the Corporation.

8. The eighth part of the document is a list of the names of the persons who have been appointed to the various positions of the Board of Directors of the Corporation.

9. The ninth part of the document is a list of the names of the persons who have been appointed to the various positions of the Board of Directors of the Corporation.

10. The tenth part of the document is a list of the names of the persons who have been appointed to the various positions of the Board of Directors of the Corporation.

11. The eleventh part of the document is a list of the names of the persons who have been appointed to the various positions of the Board of Directors of the Corporation.

III. ATLAS 1 RESULTS

A. *Artificial Aurora Experiments*

Gaining an understanding of Earth's natural aurora will require a multifaceted experimental and theoretical approach. The dynamical nature of the aurora and the tendency for many important phenomena to occur together have made it difficult to determine the relative roles of the magnetosphere and the ionosphere in triggering auroral displays and in determining the sources and closure of the field-aligned currents associated with them. Measurements of the fields and plasmas associated with the aurora need to be made at higher temporal and spatial resolution, and ultimately at multiple locations simultaneously, in order to characterize sufficiently the auroral particle acceleration processes. Of particular interest is the auroral acceleration region, which is located at altitudes of an Earth radius or so along the magnetic field lines threading the aurora; sounding rockets and satellites with increased capabilities are contributing significantly to the investigation of the auroral acceleration region. A complementary approach involves the use of artificial electron beams either to stimulate auroral displays in quiet regions where an unambiguous input-output experiment can be performed or to sense remotely auroral phenomena such as parallel electric fields as they occur naturally.

Artificial electron beams from the SEPAC experiment on the ATLAS 1 Spacelab payload were used to stimulate auroral emissions at southern auroral latitudes. The emitted electron beams were monoenergetic at 6.25 keV and were fired in one-second pulses every fifteen seconds with currents of 1.21 A. Optical measurements of the beam were made in the vicinity of the Shuttle Orbiter by its on-board television camera and in the upper atmosphere by the Atmospheric Emissions Photometric Imager (AEPI). AEPI imaged auroral emissions in both white light and at the 427.8 nm N_2^+ emission line. Energy deposition calculations and the results of previous sounding-rocket experiments had suggested that emissions with scale sizes of about 130 meters would result from the artificial electron beams with the visible emissions extending from about 110 to 130 km altitudes. In the ATLAS 1 experiments the auroral imaging was performed from the Shuttle, providing a new perspective on the artificial auroras and allowing the emissions to be traced from altitudes near the 295 km Shuttle altitude down to the 110 km level along the curved magnetic field lines.

In the ATLAS 1 SEPAC artificial aurora experiments easily detectable light emissions were produced both in quiet regions and within very active auroral forms. This result suggests that future experiments may be used to detect parallel electric fields above auroras by launching artificial electron beams upward from the Shuttle and detecting light emissions produced by the reflected beams as they return to the atmosphere.

The results of the ATLAS 1 artificial aurora experiments are reported in the following publications, which are included in the Appendix:

Burch, J. L., S. B. Mende, N. Kawashima, W. T. Roberts, W. W. L. Taylor, T. Neubert, W. C. Gibson, J. A. Marshall and G. R. Swenson, Artificial auroras in the upper atmosphere: 1. electron beam injections, *Geophys. Res. Lett.*, 20, 491-494, 1993.

Mende, S. B., J. L. Burch, G. R. Swenson, E. K. Aamodt, S. P. Geller, R. L. Rairden and P. L. Hassler, Artificial auroras in the upper atmosphere: 2. imaging results, *Geophys. Res. Lett.*, 20, 495-498, 1993.

Burch, J. L., W. T. Roberts, W. W. L. Taylor, N. Kawashima, J. A. Marshall, S. L. Moses, T. Neubert, S. B. Mende and E. Y. Choueiri, Space experiments with particle accelerators: SEPAC, *Adv. Space Res. (The Earth's Middle Atmosphere)*, 14, 263-270, 1994.

B. Critical Ionization Velocity Experiments

The critical ionization velocity (CIV) theory states that neutral gas traveling perpendicular to a magnetic field will suddenly become ionized when its velocity in the rest frame of the magnetic field reaches a threshold value such that the kinetic energy of the gas in that frame is equal to its ionization potential. The CIV phenomenon has been suspected to play an important role in various plasma dynamics situations ranging from cometary comas and astrophysical problems to spacecraft environment interactions. While CIV has been observed in many laboratory experiments, a definitive and unambiguous observation of this phenomenon in space has not been made.

A test of the CIV theory was made with neutral xenon releases from the SEPAC hollow cathode plasma contactor onboard the ATLAS 1 payload. The gas velocity perpendicular to the Earth's magnetic field was essentially the orbital velocity (7.5 km/s), and thus it exceeded the CIV for xenon. The releases were observed with onboard instrumentation. A factor of 60 enhancement was seen in the Langmuir probe current. Calculations confirmed that release conditions generally satisfied criteria for CIV and predicted a maximum factor of 20 increase in plasma density. Thus CIV effects were likely to have occurred during the ATLAS 1 experiments. The results of these experiments are documented in the following paper, which is included in the Appendix:

Marshall, J. A., J. L. Burch, E. Y. Choueiri and N. Kawashima, CIV experiments on ATLAS 1, *Geophys. Res. Lett.*, 20, 499-502, 1993.

C. Plasma Contactor Operations

SEPAC on ATLAS 1 included a plasma contactor to neutralize charge buildup on the orbiter due to electron accelerator operations. The SEPAC plasma contactor operated the same as it had during testing in the laboratory in that it emitted currents that helped balance the electron beam current. The Langmuir probe measured the charge exchange ions and the thermal electrons emitted by the contactor. The electric field wave data showed an order of magnitude increase in the 4-8 MHz band. There were no reports of contactor operations interfering with either orbiter systems or other ATLAS 1 experiments.

The results of the SEPAC plasma contactor operations are documented in the following publication, which is included in the Appendix:

1. The first part of the document is a letter from the President of the United States to the Congress, dated January 1, 1861.

2. The second part is a report from the Secretary of the Treasury, dated January 1, 1861.

3. The third part is a report from the Secretary of the Interior, dated January 1, 1861.

4. The fourth part is a report from the Secretary of the Navy, dated January 1, 1861.

5. The fifth part is a report from the Secretary of the War, dated January 1, 1861.

6. The sixth part is a report from the Secretary of the State, dated January 1, 1861.

7. The seventh part is a report from the Secretary of the War, dated January 1, 1861.

8. The eighth part is a report from the Secretary of the Navy, dated January 1, 1861.

9. The ninth part is a report from the Secretary of the Interior, dated January 1, 1861.

10. The tenth part is a report from the Secretary of the Treasury, dated January 1, 1861.

11. The eleventh part is a report from the Secretary of the War, dated January 1, 1861.

12. The twelfth part is a report from the Secretary of the State, dated January 1, 1861.

13. The thirteenth part is a report from the Secretary of the War, dated January 1, 1861.

14. The fourteenth part is a report from the Secretary of the Navy, dated January 1, 1861.

15. The fifteenth part is a report from the Secretary of the Interior, dated January 1, 1861.

Katz, I., J. N. Barfield, J. L. Burch, J. A. Marshall, W. C. Gibson, T. Neubert, W. T. Roberts, W. W. L. Taylor and J. R. Beattie, Interactions between the SEPAC plasma contactor and the ionosphere, submitted to *J. Spacecraft and Rockets*, 1993.



APPENDIX

ARTIFICIAL AURORAS IN THE UPPER ATMOSPHERE 1. ELECTRON BEAM INJECTIONS

J. L. Burch¹, S. B. Mende², N. Kawashima³, W. T. Roberts⁴, W. W. L. Taylor⁵,
T. Neubert⁶, W. C. Gibson¹, J. A. Marshall¹, and G. R. Swenson²

Abstract. Artificial electron beams from the Space Experiments with Particle Accelerators (SEPAC) on the ATLAS 1 Spacelab payload were used to stimulate auroral emissions at southern auroral latitudes. The emitted electron beams were monoenergetic at 6.25 keV and were fired in one-second pulses every fifteen seconds with currents of 1.21 A. Optical measurements of the beam were made in the vicinity of the Shuttle Orbiter by its on-board television camera and in the upper atmosphere by the Atmospheric Emissions Photometric Imager (AEPI). AEPI imaged auroral emissions in both white light and at the 427.8 nm N₂⁺ emission line. Energy deposition calculations and the results of previous sounding-rocket experiments had suggested that emissions with scale sizes of about 130 meters would result from the artificial electron beams with the visible emissions extending from about 110 to 130 km altitudes. In the ATLAS 1 experiments the auroral imaging was performed from the Shuttle, providing a new perspective on the artificial auroras and allowing the emissions to be traced from altitudes near the 295 km Shuttle altitude down to the 110 km level along the curved magnetic field lines.

Introduction

Gaining an understanding of Earth's natural aurora will require a multifaceted experimental and theoretical approach. The dynamical nature of the aurora and the tendency for many important phenomena to occur together have made it difficult to determine the relative roles of the magnetosphere and the ionosphere in triggering auroral displays and in determining the sources and closure of the field-aligned currents associated with them. A summary of contemporary problems that define auroral physics is provided in the book by Meng et al. [1991]. Measurements of the fields and plasmas associated with the aurora need to be made at higher temporal and spatial resolution, and ultimately at multiple locations simultaneously,

in order to characterize sufficiently the auroral particle acceleration processes. Of particular interest is the auroral acceleration region, which is located at altitudes of an Earth radius or so along the magnetic field lines threading the aurora; sounding rockets and satellites with increased capabilities are contributing significantly to the investigation of the auroral acceleration region. A complementary approach involves the use of artificial electron beams either to stimulate auroral displays in quiet regions where an unambiguous input-output experiment can be performed or to sense remotely auroral phenomena such as parallel electric fields as they occur naturally.

The Space Experiments with Particle Accelerators (SEPAC) were conducted as part of the ATLAS 1 Spacelab mission from March 24 through April 2, 1992. One of the objectives was to perform artificial aurora experiments from orbit using high-power electron beams and the optical imaging capability of the Atmospheric Emissions Photometric Imaging (AEPI) instrument [Mende et al., 1992]. The SEPAC electron beam accelerator (EBA) is capable of injecting electrons with beam energies up to 6.25 keV. At this energy the perveance-limited electron gun can emit beam currents of up to 1.21 A, giving a beam power of 7.56 kW. The previous flight of SEPAC on Spacelab 1 [Obayashi et al., 1984] showed that at these levels special means of neutralizing the Shuttle spacecraft are necessary; therefore, for ATLAS 1 the SEPAC instrument complement included three 122-cm diameter conductive spheres for charge collection and a 1.6 A hollow-cathode Xe⁺ plasma contactor. The flight data show that the effectiveness of these charge neutralization devices was sufficient for injection of electron beams up to the highest beam currents available with the SEPAC EBA.

Artificial auroral experiments had been conducted previously from sounding rockets [Hess et al., 1971; Davis et al., 1971, 1980; O'Neil et al., 1979]. See also the comprehensive review by Winckler [1980]. The results of the previous experiments led to the expectation that the SEPAC EBA, at highest power, would produce an artificial aurora characterized by an emission with a diameter of about 130 m at altitudes of 110-130 km. However, because of the favorable viewing geometry from orbit, the artificial aurora emissions produced by SEPAC on ATLAS 1 were imaged over the full extent of the curved magnetic field lines from near the Shuttle altitude of 295 km down to the 110-130 km altitude regime. Also present in the images were afterglows, which appeared as emission "tails" in the wake direction. Contrasts between SEPAC and the previous experiments include the facts that (1) the optical measurements were made from the same spacecraft from which the electron beam was injected rather than from the ground or aircraft, (2) effective charge neutralization was accomplished with the charge-collection spheres and the plasma contactor; and (3) the artificial auroras were produced in the auroral zone and in the neighborhood of natural auroras.

¹Southwest Research Institute, San Antonio, Texas
²Lockheed Palo Alto Research Laboratory, Palo Alto, California
³Institute of Space and Astronautical Science, Tokyo, Japan
⁴NASA, Marshall Space Flight Center, Alabama
⁵Nichols Research Corp., Arlington, Virginia
⁶University of Michigan, Ann Arbor, Michigan

Experiment Description

SEPAC is a joint U.S.-Japan investigation of the interaction of electron beams, plasma and neutral gas with the Earth's upper atmosphere, ionosphere and magnetosphere. It makes use of the large mass, volume and power capabilities of Shuttle/Spacelab as well as the interactive control that is possible through the involvement of payload and mission specialists. The first flight of SEPAC was with the Spacelab 1 mission (STS 9) in late November and early December 1983. Recently an upgraded instrument complement was included as part of the ATLAS 1 payload on STS-45 in late March and early April 1992. Table 1 shows the SEPAC instrument complement as flown on the ATLAS 1 payload.

During the artificial aurora experiments the plasma contactor (PC) was operated continuously so that up to 1.6 A of Xe^+ ions could be ejected to balance an equal current of electrons from the EBA. Since for ATLAS 1 the EBA current was limited to 1.21 A, the PC had more than sufficient output current capability to maintain charge neutrality during the most intense electron beam injections. The neutralization process was aided by the charge collection spheres and the Shuttle conductive surfaces (the engine bells and the inner surfaces of the payload bay doors), which can effectively collect ionospheric electrons along magnetic field lines.

Figure 1 demonstrates the ability of the plasma contactor and the conductive spheres to neutralize the Shuttle/Spacelab during electron beam injections. Figure 1 shows the spacecraft potential as measured by the three floating probes, the EBA current and voltage, and the PC current. The floating-probe data in Figure 1 show that the spacecraft potential did not rise more than about 5 V during the beam firings. By contrast, with no PC or conducting spheres on Spacelab 1, charging to the beam potential was observed when the beam current was above 100 mA [Burch, 1986].

Also providing evidence of spacecraft neutralization and of the fact that any beam-plasma instabilities or discharges did not disrupt the beam significantly during the artificial aurora experiment is the image of the beam in Figure 2. This image was taken in white light by the onboard low-light television system provided by the Shuttle Orbiter. The beam was not visible in the TV data except when neutral xenon was released from the PC. Figure 2 clearly shows the first spiral of the beam in the geomagnetic field as the beam was fired upward at 5 keV and 500 mA. The dark central segment of the straight section of the beam was produced by saturation of the TV camera, indicating the most intense part of the beam. The spiral in Figure 2 is located about 50 meters above the Shuttle. During this particular beam firing, magnetic deflection coils were used to deflect the beam by about 17° to a pitch angle near 10° resulting in the beam spiral. The divergence full angle of the beam itself was about 5° . It is possible that the injection of neutral xenon, which was required to make the beam visible to the Shuttle imager, modified the ambient environment and affected the threshold for certain beam-plasma interactions. During the artificial aurora experiments the neutral xenon injection was not employed.

Artificial Aurora Experiment

In each of the two artificial aurora experiments that were performed on ATLAS 1, twenty electron beam pulses were

Table 1. SEPAC Instrumentation for ATLAS 1

<i>Instrument/Parameter</i>	<i>Range</i>
<i>Electron Beam Accelerator (EBA)</i>	
Energy	0 to 6.25 keV
Current	0 to 1.21 A
Perveance	$2.5 \times 10^{-6} \text{ AV}^{-1.5}$
Initial Beam Diameter	20 mm
Deflection	0 to 30° from axis
Modulation	$\leq 5 \text{ kHz}$
<i>Xenon Plasma Contactor (PC)</i>	
Ion-electron production rate	1.6 A
Operation time available	1500 hrs.
Neutral gas pulse width	100 ms (programmable)
Number of ejected atoms	$\sim 6 \times 10^{22}$ per pulse
<i>Low-frequency plasma wave probe</i>	
Frequency	0.75 to 10 kHz
<i>High-frequency plasma wave probe</i>	
Frequency	0.1 to 10.5 MHz
<i>Wideband plasma wave probe</i>	
Frequency	0.4 to 10 kHz
Frequency	0.1 to 4.2 MHz (or 4.0 to 7.5 MHz)
<i>Floating probes</i>	
Distances from pallet	290 mm, 540 mm, 790 mm
Frequency	0 to 400 Hz
Potential	-8 kV to +8 kV
Resolution	6 V
<i>Energetic Electron Analyzer</i>	
Energy	0.1 to 15 keV
Energy resolution	$\Delta E/E = 0.18$
Angular acceptance	4° by 10°
Sample rate	100 Hz
Energy sweep time	320 ms
<i>Langmuir probe</i>	
Density	10^4 to 10^8 e cm^{-3}
Temperature	600 to 5000 °K
Sample rate	1 kHz (current) 250 Hz (voltage)
<i>Ionization gauge</i>	
Pressure range	5×10^{-8} to 5×10^{-4} Torr
Sample rate	1 kHz

injected downward from an altitude of 295 km with 0° pitch angle at relatively high southern magnetic latitudes (65 – 67°). During the experiments, optical observations were made with the AEPI instrumentation. In the first experiment white-light images were acquired at a rate of 30 Hz, while in the second experiment these high-rate white-light images were supplemented by images at 427.8 nm, which were integrated over 1 second. The 427.8 nm N_2^+ line was chosen because it is a prompt emission with a well-known relationship to total precipitating electron energy flux. The electron beam pulses were injected once every 15 seconds at the maximum energy and current (6.25 keV, 1.21 A) with pulse widths of 1 second.

Figure 3 shows two consecutive 427.8 nm images that were obtained 30 seconds apart in the southern auroral zone during the second artificial aurora experiment. High-time-resolution white-light images of the artificial aurora are discussed by Mende [1992]. In Figure 3a the artificial aurora

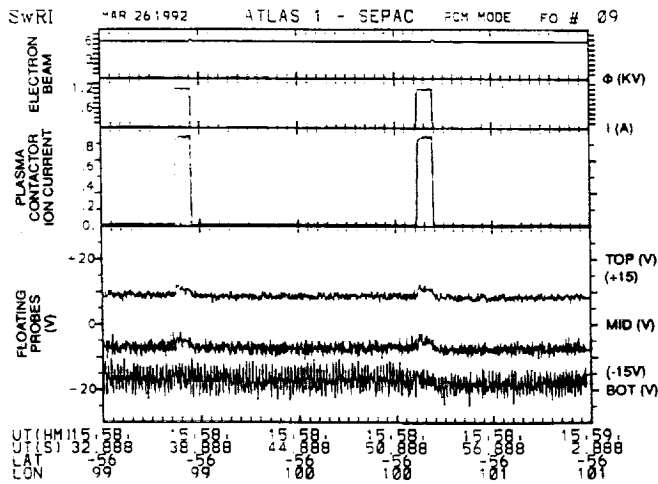


Fig. 1. A 30-second plot of the EBA voltage and current, the PC ion current, and the three floating-probe potentials in the top to bottom panels, respectively. The PC ion current is plotted in normalized units pending final monitor calibration. The floating-probe potential traces are separated by 15 V to avoid overlap.



Fig. 2. Image from an Orbiter payload-bay television camera (40° horizontal field of view) of a SEPAC artificial electron beam with energy of 5 keV and current of 500 mA. The beam was rendered visible by the injection of a neutral Xe pulse (see Table 1), which was excited by the electron beam. The dark central region of the straight section of the beam is a saturation effect. The first spiral of the beam in the Earth's magnetic field, which is evident near the end of the visible beam in the right-hand side of the figure, was located about 50 meters above the Orbiter. The illuminated object in the lower right-hand corner of the image is part of the payload bay instrumentation.

is located in the dark region near a quiet auroral arc, while in Figure 3b the artificial aurora is superimposed upon a naturally occurring quiet auroral arc. Each artificial aurora image contains significant spatial structure, the most persistent features being a tapered extension toward the bottom of the image and (particularly noticeable in Figure 3a) a trail in the Shuttle wake direction, possibly indicating an afterglow phenomenon. The travel time of the beam to the 110 km level

is only about 5 ms, and the 427.8 nm emission is prompt, with a lifetime of $<1 \mu\text{s}$; therefore, the wake trail was not predicted. The afterglow present in the wake trail may have been produced by induced electron precipitation, caused perhaps by an enhancement of ionospheric Pederson conductivity produced by the artificial beams, although this possibility needs to be investigated further. Another possibility is the acceleration of ambient electrons by beam-plasma interactions that may have persisted for several tens of ms after the electron beam moved out of an excited magnetic flux tube, as suggested by Wilhelm et al. [1985].

The tapered extensions toward the bottom of the images in Figures 3a and 3b are produced by the curvature of the

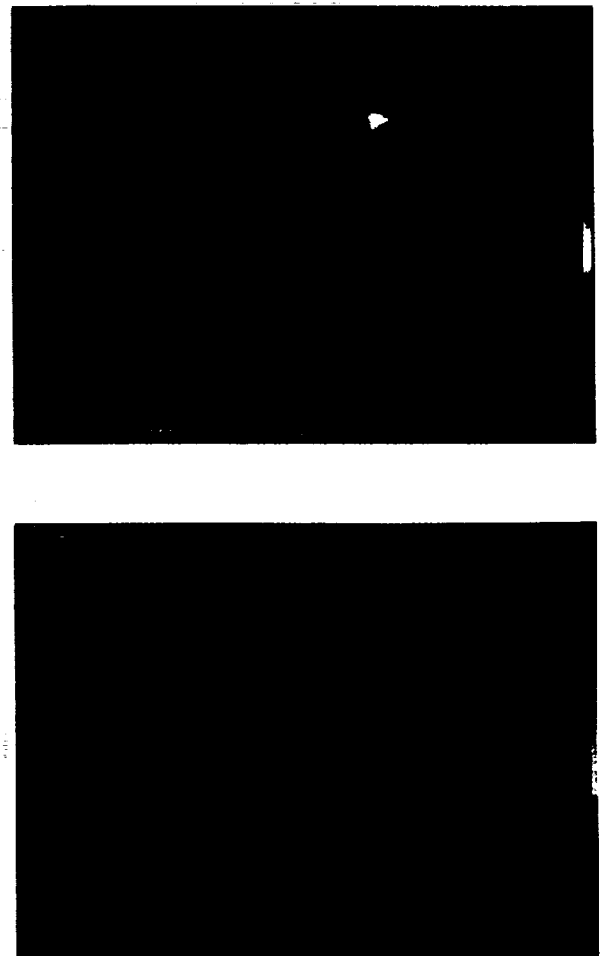


Fig. 3. (a) Artificial aurora image in 427.8 nm. To the left is a quiet auroral arc; in the upper right is the artificial aurora. The image was obtained by the AEPI instrument [Mende et al., 1992], which viewed downward along the magnetic field direction, during a one-second period beginning at 16:01:59 UT on March 26, 1992. The direction of motion of the Shuttle Orbiter was to the left, so the natural auroral arc is broadened in the horizontal direction by about 10%. The width of the image at the 110-km level is about 80 km. The color bar is linear from top to bottom and extends from 0 to about 5 kR. (b) Same as (a) except that in this case the image was obtained over the one-second period beginning at 16:02:29 UT on March 26, 1992, and the artificial aurora was superimposed upon a somewhat weaker quiet auroral arc.

magnetic field line. For this experiment the Shuttle was moving generally eastward, or to the left in figures 3a and 3b, so south and north are toward the top and bottom of the figures, respectively. The AEPI has a field of view of 20° , so at 110 km the width of the images in Figure 3 is about 80 km. The displacement of a dipole field line at a magnetic latitude of 65° between 295 km and 110 km because of field-line curvature is about 1.8 km, which is consistent with the images in Figure 3. The bottom tip of the downward tapered extensions in Figure 3 is, then, the lower extension of the artificial aurora at altitudes of about 110 km. Detailed analysis of the images is reported by Mende et al. [1992].

Future experiments are needed to take advantage of the much greater detectability of the artificial aurora emissions from orbit in performing more extensive spectral analyses and in using the artificial electron beams to sense remotely electric fields in the auroral zone. For example, the use of an oxygen emission line (such as 630.0 nm) along with the nitrogen line would help determine the altitude profile of the artificial aurora. In addition, the fact that the artificial auroras are easily detectable even when superimposed on bright natural auroras supports the possibility that upward-propagating electron beams, reflected by parallel electric fields above the aurora, would produce detectable artificial auroras, which could be used to map the strength and spatial distributions of the parallel E-fields.

Acknowledgements. Many people have contributed to the SEPAC experiment over the years. Professor Tatsuzo Obayashi, who is recently deceased, was the original principal investigator beginning in 1976. Bill Tomlinson and George Ferguson of SwRI and Randy Bounds of Nichols Research contributed extensively to the hardware and software efforts. At ISAS numerous scientists and engineers contributed to SEPAC, including Drs. K. Kuriki, M. Nagatomo, K. Ninomiya, and M. Ejiri. We have benefitted greatly from the involvement of co-investigators Drs. Rick Chappell and Peter Banks; the ATLAS 1 crew; the ATLAS Project personnel, under the guidance of Tony O'Neill of MSFC, and Dr. Bob Beattie of Hughes Research Laboratory. This work was supported by NASA Contracts NAS8-32488 and NAS8-32827 with SwRI.

References

- Burch, J. L., Space plasma physics results from Spacelab, *J. Spacecraft and Rockets*, 23, 331-335, 1986.
- Davis, T. N., et al., Artificial aurora experiment: ground-

based optical observation, *J. Geophys. Res.*, 76, 6082-6092, 1971.

Davis, T. N., et al., Artificial aurora conjugate to a rocket-borne electron accelerator, *J. Geophys. Res.*, 85, 1722-1728, 1980.

Hess, W. N., et al., Artificial auroral experiment: experiment and principal results, *J. Geophys. Res.*, 76, 6067-6081, 1971.

Mende et al., Artificial auroras in the upper atmosphere: 2. imaging results, *Geophys. Res. Lett.*, this issue, 1992.

Meng, C.-I., M. J. Rycroft, and L. A. Frank, *Auroral Physics*, Cambridge University Press, Cambridge, 1991.

Obayashi, T., et al., Space experiments with particle accelerators, *Science*, 225, 195-196, 1984.

O'Neil, R. R., E. T. P. Lee, and E. R. Huppi, Auroral O(1S) production and loss processes: ground-based measurements of the artificial auroral experiment Precede, *J. Geophys. Res.*, 84, 823-833, 1979.

Rees, M. H., G. J. Romick, H. R. Anderson, and R. T. Casserly, Jr., Calculation of auroral emissions from measured electron precipitation: comparison with observation, *J. Geophys. Res.*, 81, 5091-5096, 1976.

Wilhelm, K., W. Bernstein, P. J. Kellogg, and B. A. Whalen, Fast magnetospheric echoes of energetic electron beams, *J. Geophys. Res.*, 90, 491-504, 1985.

Winckler, J. R., The application of artificial electron beams to magnetospheric research, *Rev. Geophys. Space Phys.*, 18, 659-682, 1980.

J. L. Burch, W. C. Gibson, and J. A. Marshall, Southwest Research Institute, P. O. Drawer 28510, San Antonio, TX 78228-0510.

S. B. Mende and G. R. Swenson, Lockheed Palo Alto Research Laboratory, 3257 Hanover Street, Palo Alto, CA 94304.

N. Kawashima, Institute of Space and Astronautical Science, Sagami-hara, Kanagawa 172, Japan.

W. T. Roberts, PS02, Marshall Space Flight Center, Alabama 35812.

W. W. L. Taylor, Nichols Research Corp., 1700 N. Moore St., Arlington, VA 22209.

T. Neubert, Space Physics Research Laboratory, University of Michigan, Ann Arbor, MI 48109.

(Received: September 21, 1992;
revised: January 28, 1993;
accepted: January 29, 1993)

ARTIFICIAL AURORAS IN THE UPPER ATMOSPHERE: 2. IMAGING RESULTS

S. B. Mende¹, J. L. Burch², G. R. Swenson¹, E. K. Aamodt¹,
S. P. Geller¹, R. L. Rairden¹ and P. L. Hassler³

Abstract. On the ATLAS 1 mission (STS-45, launched March 24, 1992) two experiments, AEPI (Atmospheric Emissions Photometric Imaging) and SEPAC (Space Experiments with Particle Accelerators) performed the first experiment in a series of active experiments intended to probe the atmosphere, ionosphere and magnetosphere with electron beams. The luminous artificial aurora generated by the electron beam interaction was detected and measured by AEPI both in white light and in a narrow wavelength band at 427.8 nm (peak intensity 5 kR). Modelling calculation showed that there was a significant contribution from emissions originating near the spacecraft. The spatial intensity distribution of the observed auroral patch is consistent with emission contribution from both high and low altitude regions. An extended tail in the direction of the shuttle wake was observed in the 427.8 nm channel, consistent with a decay time associated with the dissipation of the hot electron plasma.

Introduction

One of the key questions in understanding magnetospheres is the mapping of the instantaneous position of the magnetic field. From a theoretical standpoint, artificial electron beams are ideal for tracing magnetic fields. Energetic electrons have very short transit times compared to the time scale of the changes in the magnetic field. The electron trajectories are perturbed only by electromagnetic effects such as gradient and curvature and $E \times B$ drift. By varying the electron energy and pitch angle, in principle, one can separate any of these effects. There were several previous rocket experiments in which optical emissions or artificial auroras were generated successfully [Hess et al., 1971; Davis et al., 1971, 1980; Cambou et al., 1975, 1980; Hallinan et al., 1978, 1990; O'Neil et al., 1978a, 1978b, 1979]. The signal to noise ratio of the artificial auroras produced by these rocket-borne accelerator experiments were generally low. It seemed that electron accelerators suitable for spacecraft-based magnetospheric electron beam probing would have to be very large and powerful. One of the most successful rocket experiment series, the Echo experiments [Hendrickson et al., 1976; Winckler, 1982; Malcolm, 1986; Winckler et al., 1989], detected echoes returned from conjugate hemispheres by electron detectors on the same rocket which carried the electron accelerator.

A second objective of these artificially injected electron beam experiments is the investigation of the aeronomical processes created when an electron beam of known characteristics interacts with the atmosphere [O'Neil et al., 1978a, 1978b; O'Neil et al., 1979].

A shuttle-borne particle accelerator and optical detector were flown on the ATLAS 1 shuttle mission (STS-45) at an

altitude of 300 km. Artificial auroral experiments were conducted on this mission with positive results [Burch et al., 1992]. In this paper the optical observations of the artificially induced auroras by the Atmospheric Emission Photometric Imaging (AEPI) experiment will be described.

AEPI Experiment Description

The AEPI experiment [Sandie et al., 1983] was developed originally for the Spacelab 1 (STS-9) shuttle flight and was first flown in November 1983. The instrument consisted of a shuttle bay mounted instrument package which was operated remotely by the crew through the AEPI control panel which was installed inside the shuttle's manned environment. AEPI was essentially a remote-sensing optical instrument mounted on a two axis gimbal, which could be pointed independently from the orientation of the shuttle.

There were two separate imagers inside the optical package. The filtered camera had a dual filter wheel providing wavelength selection with a minimum bandwidth of ~ 2 nm. The detector contained an image intensifier, which was fiber-optically coupled to a CCD. The CCD was thermoelectrically cooled and operated in the low dark current MPP (multi pinned phase) mode. This camera was capable of taking long time-exposures (several seconds). The second detector was a white light (spectral continuum) camera, which had a wavelength response between 430 and 850 nm (but contained a 762 nm notch filter to suppress airglow). This detector operated at standard TV frame rates (30 frames per second) with a fixed 1/30 second integration.

AEPI had only one video line, and the two cameras time-shared the line. The general properties of the AEPI experiment detectors are summarized in Table 1.

All ancillary parameters including frame count, UT, filters, image intensifier gain, filtered camera exposure time, pointing angles with respect to the shuttle and to a fixed point geographic reference, magnetic field vector, solar elevation and latitude/longitude of the shuttle orbiter were superimposed on the image (Figure 1).

The ATLAS-1 Artificial Aurora Experiments

The AEPI gimbal pointed the optical axis approximately parallel to the magnetic field. During the AEPI-SEPAC joint experiments, the electron accelerator produced a sequence of pulses of 1 second duration, each at a rate of 1 pulse every 15 seconds. Each sequence lasted 5 minutes. In order to neutralize the shuttle and inhibit its positive charging, the SEPAC experiment [see Burch et al., 1992] operated a plasma contactor, which released a stream of xenon ions from a hollow cathode ion source. During the first AEPI-SEPAC artificial aurora experiment, only the AEPI continuum TV camera operated and only white light images of the electron beam were recorded. During the second joint experiment opportunity, the artificially induced auroral emissions were recorded by both the filtered and unfiltered AEPI imagers. In the AEPI filtered camera the selected filter was centered at 427.8 nm and had a bandwidth of 2.2 nm. The camera operation mode consisted of an exposure for approximately 1 second. Although the capability to synchronize SEPAC and AEPI existed, during these test firings the two instruments operated independently, and the one second duration electron pulses were mostly picked up by two consecutive read out

¹ Lockheed Palo Alto Research Laboratories, Palo Alto, CA

² Southwest Research Institute, San Antonio, TX

³ NASA Marshall Space Flight Center, Huntsville, AL

Copyright 1993 by the American Geophysical Union.

Paper number 93GL00594

0094-8534/93/93GL-00594\$03.00

Table 1. AEPI Imagers

	Filtered camera (operated with 427.8 nm filter)	Unfiltered continuum camera (notch suppression at 762 nm)
Spectral bandwidth:	2.2 nm	430-850 nm
F-number:	2.0	0.95
F.O.V. (horizontal)	20°	22°
F.O.V. (vertical)	15°	16°
Frame rate:	30 to 1/30 s ⁻¹ (variable time rate)	30 s ⁻¹

frames. A typical aurora patch image, acquired at 86/16:00:14 UT by the filtered camera in 427.8 nm, is shown in Figure 1. The inset shows the relevant portion of a simultaneous image taken by the continuum camera (1/30 sec exposure). The low contrast in the white light image is largely due to some yet unexplained glow which occurs only during beam firing in the immediate neighborhood of the shuttle. In the filtered camera this glow is largely absent and the electron beam induced emissions show up as well defined auroral patches.

It is known that when an aurora is viewed from the ground up in a direction along the magnetic field line, the ratio between the integrated 427.8 nm column emission intensity and the precipitated electron energy flux is about 200 Rayleighs per erg cm⁻² sec⁻¹ [Rees et al., 1976]. The SEPAC pulses of 6.25 keV and 1.21 ampere deposited a total power of 7.6 kilowatt = 7.6×10^{10} erg sec⁻¹, which would create an aurora of 1.6×10^{13} R cm² for a ground based observer. Since the optical resolution element of the AEPI instrument was of the order of about 1 km² = 10^{10} cm² when projected to the 100 km altitude region, one might have expected to detect 1.6 kR emission concentrated in one single resolution element (pixel). In fact, the auroral patch was substantially larger than one pixel and the measured intensity in the peak of the patch was 5 kR (Figure 2).

The presence of the greater intensity in the central pixel, and the fact that the spot was considerably larger than a single pixel, suggests that there was a substantial contribution from regions closer to the shuttle. In order to calculate the expected intensity we have considered a simple model of the electron beam, in which the imager is considered to be looking (downward parallel to a straight magnetic field line) along the center of a uniform electron beam. The central pixel is looking

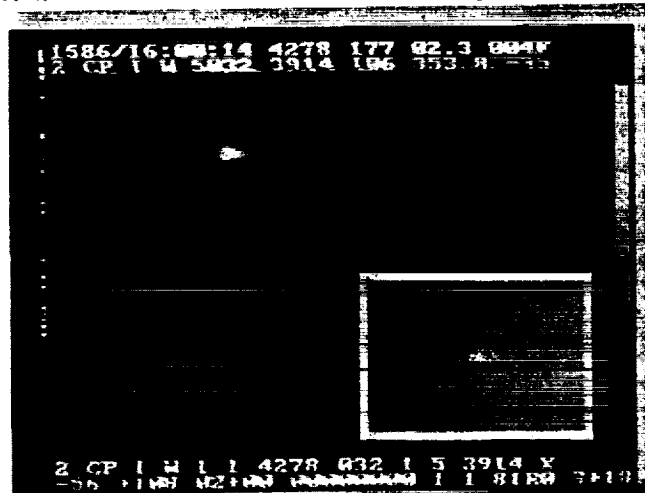


Fig. 1. An example of the artificial aurora patch imaged with the 427.8 nm filter. The inset shows the same patch in white light from the continuum camera. Both images show the existence of a luminous tail in the wake direction. The contrast in the white light image is relatively low because of near field luminosity stimulated by the electron beam. The filtered image appears to be larger and less symmetric in the up and down direction.

directly along the axis of the cylinder, and collects light emissions which can be considered to be the sum of emissions from two regions. The first region, nearest to the imager, is entirely contained within the cylinder. Emissions occurring in this region can be computed simply by integrating the volume emission rate along the line of sight. Light collection from the other more distant region is subject to the inverse square law attenuation. In our model, we performed the integration of intensity contribution into the central pixel from both regions. The other pixels adjacent to the central one were calculated simply without regard to the inverse square attenuation. We realize that this model is greatly simplified. In reality, the electron emission did not produce a uniformly luminous cylinder since the magnetic field is curved.

The electron beam in the model had the same energy flux as the SEPAC beam. In the four cases considered the diameter, *D*, of the uniformly distributed electron beam was set to 5, 10, 50 and 150 meters. A simple model atmosphere of Rees et al. [1976] was used with a 5.3×10^{-18} cm² cross-section for N₂⁺ 427.8 nm production [Vallance-Jones, 1974]. In our model the emphasis was on the contribution of the high altitude atmosphere interaction; therefore, a relatively simple modeling of the primary interaction was satisfactory. Nevertheless our simple model gave good agreement with earlier studies. For example, in our model, a one erg cm⁻² electron beam of 6250 eV electrons produced an integrated column intensity of 200 Rayleighs, in agreement with the more sophisticated modelling, e.g., Rees et al. [1976]. Our model produced the volume emission rate as a function of altitude shown on Figure 3 as a dashed curve.

The result of our model in which the distant regions are weighted with the inverse square law is also shown in Figure 3 (solid line). For the curve shown, a beam diameter of 10 m was selected which is equivalent to a uniform electron flux of 8×10^{12} electrons s⁻¹ cm⁻². The abscissa is the apparent

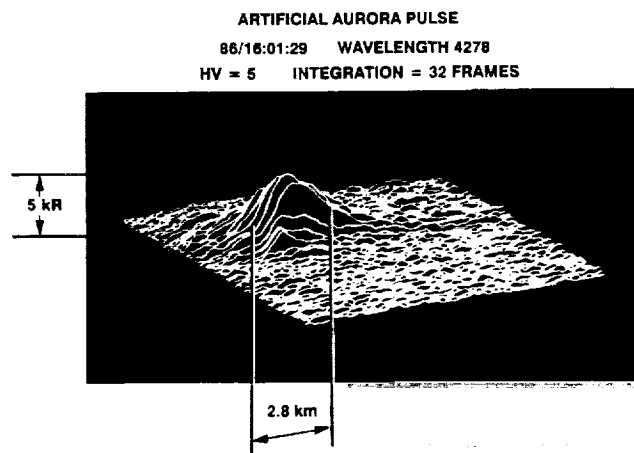


Fig. 2. Artificial aurora pulse observed through a 427.8 nm filter at 86/16:01:29 displayed as an intensity perspective plot. The field line curvature would displace the auroral "hot spot" originating in the 100-140 km region downward (to the lower left) in the plot. The 2.8 km dimension is for far field (low altitude).

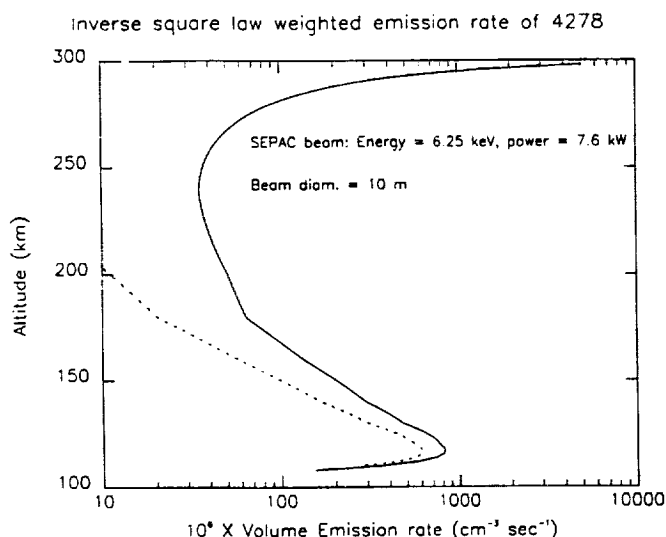


Fig. 3. Apparent volume emission rate profiles given by the simple model. Broken line shows no inverse square law correction. Solid line shows the apparent volume emission rate normalized to fill one resolution element of the imager as observed from the orbit. The normalization is equivalent to applying inverse square law correction for the distance between the emitting region and the observer viewing straight down the electron beam.

volume emission rate given in 10^6 photons $\text{cm}^{-3} \text{sec}^{-1}$. One can see from Figure 3 that the emissions produced in the high altitude region closer to the observer are a significant component when compared to the inverse square law attenuated 10 meter diameter emission spot originating in the lower atmosphere. The total column sum of the emission is 4.5 kR. This value should be compared to 1.6 kR, which would be the expected intensity if the SEPAC beam had produced its emission only in the 110 km altitude region. The results of modelling the different beam diameters are summarized in Table 2.

The first column shows the beam diameter chosen for the calculation. The integrated sum of the intensity in the distant region subject to the inverse square law is shown in the second column. The contribution to Pixel 1 from the region close to the observer is summarized in column 3. Column 4 is the total contribution to Pixel 1. Column 5 and 6 are the contributions to the adjacent pixels, Pixel 2 and Pixel 3, respectively. Small beam diameters lead to relatively large contributions by the emissions close to the orbiter.

In the realistic case, which considers the field line curvature, the central "hot spot" in the 110 km atmosphere is displaced by 1.7 km or two pixels from the center of the electron cylinder. In addition the electron beam distribution would not be expected to be uniform in the cylinder and the electrons would be concentrated at the peripheries of the cylinder. More detailed modelling is beyond the scope of this paper.

The image shown on Figure 2 shows that the central brightest region is displaced in the downward direction, in agreement with the expected sense of the displacement, because the field line curvature at the geographic location of the observer would displace the "hot spot" originating in the lower atmosphere in the downward direction on the image.

During the ATLAS-1 mission, we had several occasions during which star fields were observed. From such in-flight calibrations the angular calibration corresponding to the size of a pixel was obtained. The technique was also used to obtain the point source response, spatial resolution element or pixel size of the instrument. The intensity calibrations were corroborated by the measurement of the absolute response of the instrument to known stars.

The intensity of the pulses detected in the 427.8 nm channel was interpreted using pre-, post-, and in-flight calibrations. The postflight calibration showed no significant

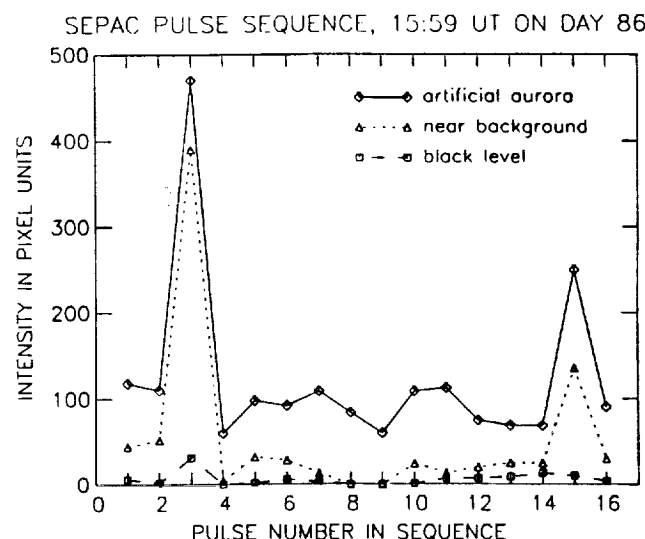


Fig. 4. The time history of the 427.8 nm emission intensities as measured during the second AEPI-SEPAC artificial auroral experiment. This experiment was performed in the auroral ionosphere and there were active auroras at times in the background.

sensitivity difference. Thus we are confident that the intensity of the central pixel of the artificial aurora pulse at 16:01:29 UT was 5 kR.

The existence of a tail-like decay in the white light camera image (Figure 1 inset) was expected because in this channel some of the spectral components have long lived upper states exhibiting long decay. For example, the 557.7 nm O^1S (lifetime of 0.74 seconds) would produce a tail consistent with the observed (6 km) length. The observation of a tail in the filtered 427.8 nm emission (lifetime < 1 ms) was unexpected. Since the electron beam and the observer are moving with the same speed, a spontaneously emitting emission should produce a spot that closely tracks the electron beam interaction region and was, therefore, expected to be a small round spot. The existence of a tail is evidence for a finite decay time. This finding is consistent with the "prompt responses" observed by Wilhelm et al. [1985], who found evidence that the lifetime of energetic electrons is several hundred milliseconds in the vicinity of the electron beam generator and that the decay time is a characteristic of the beam plasma discharge effect ignited by the electron beam. It should be noted that any form of temporal decay in the intensified CCD imager cannot cause such an artifact because the tail is spatially displaced from the main bright spot on the detector. Furthermore it should be noted that when the AEPI CCD is substantially overloaded it tends to produce vertical, and not horizontal, streaks. Thus the observed horizontal tail is not an artifact of the observing instrument.

As we have discussed, the apparent intensity of individual artificial aurora pulses varied greatly because of the lack of time synchronization between the start of the one second electron beam pulse and the one second exposure duration. It was found that much of the intensity variation could be removed by simply summing consecutive pulses. For the sequence of artificial electron pulses the intensity corrected

Table 2. Artificial Aurora Model Properties.
Column Integrated Emissions.

	First pixel		2nd pix	3rd pix
	Region 1	Region 2	sum	
	Inverse Square	No Inverse	(R)	(R)
(m)	(R)	(R)	(R)	(R)
5	7700	2700	10400	1380
10	4500	1380	5880	460
50	3040	290	3330	140
150	2890	38	2928	32

aurora patches are shown in Figure 4. During this sequence there were some natural auroras in the field of view. Most of the fluctuations in intensity were due to natural auroras which were present as a variable background. This intensity of this background was measured from the images as the video signal of the approximately uniform region in the vicinity of the artificial aurora pulses. The time plot of this background is shown on Figure 4 as the middle curve. The third curve, the rectangles on Figure 4, represent the intensity of the darkest pixels in the images. From this plot it is evident that the auroral spots appear to be superimposed on a variable background. We did not find a dependence of the intensity of the artificial aurora pulses on the intensity of the local natural aurora.

The continuum camera instrument permitted studying the time development of the intensity of individual artificial auroral pulses with a time resolution of 1/30 sec. The duration of the SEPAC pulse is 1 second. From these studies we noted that there was an enhancement in the background light during the occurrence of the artificial aurora. This enhancement began simultaneously with the start of the electron beam emission probably due to the camera seeing the enhancement in the plasma close to the orbiter. Nine television frames (about 300 ms) after the initiation of the beam there was a large intensification of this background. Plots were made for several artificial auroral pulses and they all showed to some degree the changes in background intensity in the vicinity of the artificial aurora. The relative uniformity of the time dependent background level is evidence that a discharge phenomena occurs in the orbits immediate vicinity which has a definite onset time during the 1 second beam firing.

Conclusion

During the ATLAS mission the SEPAC experiment emitted 7.5 kW electron beams with a 1-second duration. The AEPI instrument detected the artificial auroras and measured their spatial extent, intensity and time profile. Relatively simplistic modeling of the electron beam and the observing geometry showed that in addition to the classical auroral patch emitted from 110 km altitude auroral atmosphere below the orbiter there is another significant component coming from the beam interacting with the nearby atmosphere. Because of the relatively small spatial extent of the artificially produced auroral light collected from the lower atmosphere, it is attenuated by the inverse square law. The intensities of the artificial aurora pulses were measured, and they appear to be in agreement with the intensity produced by a simple model which included both the emissions which are generated nearby (1 - 2 km) and those which are produced far away (140 - 180 km) from the shuttle orbiter. The expected emission intensity calculation is based on a simple model of uniform cylindrical electron beam interacting with the atmosphere where well established 427.8 nm production rates, atmospheric models the total energy of the SEPAC beam were used.

The auroral patches appeared to be spatially elongated in the wake direction which represents a temporal decay. This observation was made in the 427.8 nm N_2^+ first negative band which is known to have a lifetime which is very short. The emission intensity produced by the artificially created auroral spots did not change noticeably when the spots were superimposed on natural auroras.

The shape of the luminous patches shows a distinct asymmetry due to the displacement of the lower atmospheric emission "hot spot" because of the curvature of the geomagnetic field.

The success of these observations pave the way for further active experiments using energetic electron guns and optical detection techniques from the space shuttle. These active experiments would include the study of production efficiency of different spectral components of the aurora, and the electron beam probing of the electric and magnetic field structures above the ionosphere.

Acknowledgments. The contributors to the AEPI experiment are too many to name. The authors gratefully

acknowledge contributions of the staff at the Lockheed Palo Alto Research Laboratories, NASA George C. Marshall Space Flight Center and NASA Johnson Space Center. Special thanks are due to the astronaut crew of the STS-45 (Atlas 1) mission. This research was funded by NASA under contract number NAS-8-32579.

References

- Burch, J. L., et al., *Geophys. Res. Lett.* (this issue), 1992.
- Cambou, F., et al., The Zarnitza rocket experiment on electron injection, *Space Res.*, **15**, 491, 1975.
- Cambou, F., et al., General description of the Araks experiments, *Ann. Geophys.*, **36**, 271, 1980.
- Davis, T. N., et al., Artificial aurora experiment: Ground-based optical observations, *J. Geophys. Res.*, **76**, 6082-6092, 1971.
- Davis, T. N., et al., Artificial aurora conjugate to a rocket-borne accelerator, *J. Geophys. Res.*, **85**, 1722, 1980.
- Hallinan, T. J., et al., The Echo 4 electron beam experiment: Television observation of artificial auroral streaks indicating strong beam interactions in the high-latitude magnetosphere, *J. Geophys. Res.*, **83**, 3263-3272, 1978.
- Hallinan, T. J., et al., Conjugate echoes of artificially injected electron beams detected optically by means of new image processing, *J. Geophys. Res.*, **95**, 6519-6532, 1990.
- Hendrickson, R. A., et al., Echo III: The study of electric and magnetic fields with conjugate echoes from artificial electron beams injected into the auroral zone ionosphere, *Geophys. Res. Lett.*, **3**, 409-412, 1976.
- Hess, W. N., et al., Artificial auroral experiment: experiment and principal results, *J. Geophys. Res.*, **76**, 6067, 1971.
- Malcolm, P. R., Electron Echo 6 - a study by particle detectors of electrons artificially injected into the magnetosphere, Ph.D. thesis, Univ. of Minnesota, Minneapolis, 1986.
- O'Neil, R. R., et al., Summarized results of the artificial auroral experiment, Precede, *J. Geophys. Res.*, **83**, 3273-3280, 1978a.
- O'Neil, R. R., et al., Excede 2 test, an artificial auroral experiment: Ground-based optical measurements, *J. Geophys. Res.*, **83**, 3281-3288, 1978b.
- O'Neil, R. R., et al., Auroral $O(^1S)$ production and loss processes: ground-based measurements of the artificial auroral experiment Precede, *J. Geophys. Res.*, **84**, 823-833, 1979.
- Rees, M. H., et al., Calculation of auroral Emissions from measured electron precipitation: Comparison with observation, *J. Geophys. Res.*, **81**, 5091-5096, 1976.
- Sandie, W. G., et al., Atmospheric emissions photometric imaging experiment for Spacelab 1, *Opt. Eng.*, **22**, 756-764, 1983.
- Vallance-Jones, A., *Aurora*, p. 126, D. Reidel Publishing Company, Boston, 1974.
- Wilhelm K., et al., Fast Magnetospheric echoes of energetic electron beams., *J. Geophys. Res.*, **90**, 491-504, 1985.
- Winckler, J. R., The use of artificial electron beams as probes of the distant magnetosphere, in *Artificial Particle Beams in Space Plasma Studies*, edited by B. Grandal, p. 3 Plenum, N. Y., 1982.
- Winckler, J. R., et al., Echo 7: An electron beam experiment in the magnetosphere, *Eos Trans. AGU*, **70**, 657, 1989.

J. L. Burch, Southwest Research Center, P. O. Drawer 28510, San Antonio, TX 78228-0510.

P. L. Hassler, NASA/Marshall Space Flight Center, Mail code EJ23, Huntsville, AL 35812.

S. B. Mende, G. R. Swenson, E. K. Aamodt, S. P. Geller, R. L. Rairden, Lockheed Palo Alto Research Laboratory, D91-20, B255, 3251 Hanover St., Palo Alto, CA 94304.

(Received September 21, 1992;

revised January 28, 1993;

accepted January 29, 1993)



SPACE EXPERIMENTS WITH PARTICLE ACCELERATORS: SEPAC

J. L. Burch,¹ W. T. Roberts,² W. W. L. Taylor,³
N. Kawashima,⁴ J. A. Marshall,¹ S. L. Moses,³ T. Neubert,⁵
S. B. Mende⁶ and E. Y. Choueiri⁷

¹ Southwest Research Institute, San Antonio, TX 78228-0510, U.S.A.

² NASA/Marshall Space Flight Center, Huntsville, AL 35812, U.S.A.

³ Nichols Research Corporation, Arlington, VA 22209, U.S.A.

⁴ ISAS, Tokyo, Japan

⁵ The University of Michigan, Ann Arbor, MI 48109-2143, U.S.A.

⁶ Lockheed Palo Alto Research Laboratory, Palo Alto, CA 94304, U.S.A.

⁷ Princeton University, Princeton, NJ 08544, U.S.A.

ABSTRACT

The Space Experiments with Particle Accelerators (SEPAC), which flew on the ATLAS 1 mission, used new techniques to study natural phenomena in the Earth's upper atmosphere, ionosphere and magnetosphere by introducing energetic perturbations into the system from a high power electron beam with known characteristics. Properties of auroras were studied by directing the electron beam into the upper atmosphere while making measurements of optical emissions. Studies were also performed of the critical ionization velocity phenomenon.

INTRODUCTION

The Space Experiments with Particle Accelerators (SEPAC) were conducted as part of the ATLAS 1 Spacelab mission from March 24 through April 2, 1992. One of the objectives was to perform artificial aurora experiments from orbit using high-power electron beams and the optical imaging capability of the Atmospheric Emissions Photometric Imaging (AEPI) instrument /1/. The SEPAC electron beam accelerator (EBA) is capable of injecting electrons with beam energies up to 6.25 keV. At this energy the perveance-limited electron gun can emit beam currents of up to 1.21 A. The previous flight of SEPAC on Spacelab 1 /2/ showed that at these levels special means of neutralizing the Shuttle are necessary; therefore, for ATLAS 1 the SEPAC instrument complement included three 122-cm diameter conductive spheres for charge collection and a 1.6 A hollow-cathode Xe⁺ plasma contactor. The flight data show that the effectiveness of these charge neutralization devices was sufficient for injection of electron beams up to the highest beam currents available with the SEPAC EBA. Another objective of SEPAC was to conduct neutral xenon releases from the plasma contactor (PC) to test the predictions of the critical ionization velocity theory.

EXPERIMENT DESCRIPTION

SEPAC is a joint U.S.-Japan investigation of the interaction of electron beams, plasma and neutral gas with the Earth's upper atmosphere, ionosphere and magnetosphere. It makes use of the large mass, volume and power capabilities of Shuttle/Spacelab as well as the interactive control that is possible through the involvement of payload and mission specialists. The first flight of SEPAC was with the Spacelab 1 mission (STS-9) in late November and early December 1983. Recently an upgraded instrument complement was included as part of the ATLAS 1 payload on STS-45 in late March and early April 1992. The upgraded SEPAC instrumentation is described by Burch et al. /3/. Table 1 shows the SEPAC instrument complement as flown on the ATLAS 1 payload.

PRECEDING PAGE BLANK NOT FILMED

TABLE 1 SEPAC Instrumentation for ATLAS I

Instrument	Parameter	Range
Electron Beam Accelerator (EBA)	Energy	0 to 6.25 keV
	Current	0 to 1.21 A
	Perveance	$2.5 \times 10^{-6} \text{ AV}^{-1.5}$
	Initial Beam Diameter	20 mm
	Deflection	0 to 30° from axis
	Modulation	$\leq 5 \text{ kHz}$
Xenon Plasma Contactor (PC)	Ion-electron production rate	1.6 A
	Operation time available	1500 hrs.
	Neutral gas pulse width	100 ms (programmable)
	Number of ejected atoms	$\sim 6 \times 10^{22}$ per pulse
Low-frequency plasma wave probe	Frequency	$0.75 \times 10 \text{ kHz}$
High-frequency plasma wave probe	Frequency	0.1 to 10.5 MHz
Wideband plasma wave probe	Frequency	0.4 to 10 kHz 0.1 to 4.2 MHz (or 4.0 to 7.5 MHz)
Floating probes	Distances from pallet	290 mm, 540 mm, 790 mm
	Frequency	0 to 400 Hz
	Potential	-8 kV to +8 kV
	Resolution	6 V
Energetic electron analyzer	Energy	0.1 to 15 keV
	Energy resolution	$\Delta E/E = 0.18$
	Angular acceptance	4° by 10°
	Sample rate	100 Hz
	Energy sweep time	320 ms
Langmuir probe	Density	10^4 to 10^8 e cm^{-3}
	Temperature	600 to 5000° K
	Sample rate	1 kHz (current) 250 Hz (voltage)
Ionization gauge	Pressure gauge	5×10^{-8} to $5 \times 10^{-4} \text{ Torr}$
	Sample rate	1 kHz

ARTIFICIAL AURORA EXPERIMENT

Artificial auroral experiments had been conducted previously from sounding rockets /4,5,6,7,8/. The results of the previous experiments led to the expectation that the SEPAC EBA, at highest power, would produce an artificial aurora characterized by an emission with a diameter of about 100-150 m at altitudes of 100-120 km. However, because of the favorable viewing geometry from orbit, the artificial aurora emissions were imaged over the full extent of the curved magnetic field lines from near the Shuttle altitude of 295 km down to the 110-120 km altitude regime. Also present in the images were afterglows, which appeared as emission "tails" extending up to ~1 km in the wake direction. Contrasts between SEPAC and the previous experiments include the facts that (1) the optical imaging measurements were made from the same spacecraft from which the electron beam was injected rather than from the ground or aircraft, (2) total charge neutralization was accomplished with the charge-collection spheres and the plasma contactor; and (3) the artificial auroras were produced in the auroral zone and in the neighborhood of natural auroras.

In each of the three artificial aurora experiments that were performed on ATLAS 1, twenty electron beams were injected downward from an altitude of 295 km with 0° pitch angle at relatively high southern magnetic latitudes (65-67°). During the first and third experiments, optical observations were made with the AEPI instrumentation. In the first experiment white-light images were acquired at a rate of 30 Hz, while in the third experiment these high-rate white-light images were supplemented by images at 4278 Å, which were integrated over 1 second. The electron beam pulses were injected once every 15 seconds at the maximum energy and current (6.25 keV, 1.21 A) with pulse widths of 1 second.

Figure 1 shows two 4278 Å images that were obtained about 4 minutes apart in the southern auroral zone during the third artificial aurora experiment. In Figure 1a the artificial aurora is located in the dark region near a quiet auroral arc, while in Figure 1b the artificial aurora is superimposed upon a large naturally occurring auroral arc. Each artificial aurora image contains significant spatial structure, the most persistent features being a tapered extension toward the bottom of the image and (particularly noticeable in Figure 1a) a trail in the Shuttle wake direction, possibly indicating an afterglow phenomenon. The travel time of the beam to the 110-km level is only about 5 ms, and the 4278 Å emission is prompt, with a lifetime of $< 1 \mu\text{s}$; therefore, the wake trail was not predicted. The afterglow present in the wake trail may have been produced by induced electron precipitation, caused perhaps by an enhancement of ionospheric Pederson conductivity produced by the artificial beams, although this possibility needs to be investigated further. Another possibility is a beam-plasma interaction that persists for some time after the beam is turned off [Wilhelm et al., 1985].

The tapered extensions toward the bottom of the images in Figures 1a and 1b are produced by the curvature of the magnetic field line. For this experiment the Shuttle was moving generally eastward, or to the left in Figure 1, so south and north are toward the top and bottom of the figures, respectively. The AEPI has a field of view of 20°, so at 110 km the width of the images in Figure 1 is about 80 km. The displacement of a dipole field line at a magnetic latitude of 65° between 295 km and 110 km because of field-line curvature is about 1.8 km, which is consistent with the images in Figure 1. The bottom tip of the downward tapered extensions in Figure 1 is, then, the lower extension of the artificial aurora at altitudes of about 110 km. Detailed analysis of the images is reported by Mende et al. /1/.

Future experiments are needed to take advantage of the much greater detectability of the artificial aurora emissions from orbit in performing more extensive spectral analyses and in using the artificial electron beams to sense remotely electric fields in the auroral zone. The fact that the artificial auroras are easily detectable even when superimposed on bright natural auroras supports the possibility that upward-propagating electron beams, reflected by parallel electric fields above the aurora, would produce detectable artificial auroras, which could be used to map the strength and spatial distributions of the parallel E-fields.



Figure 1a

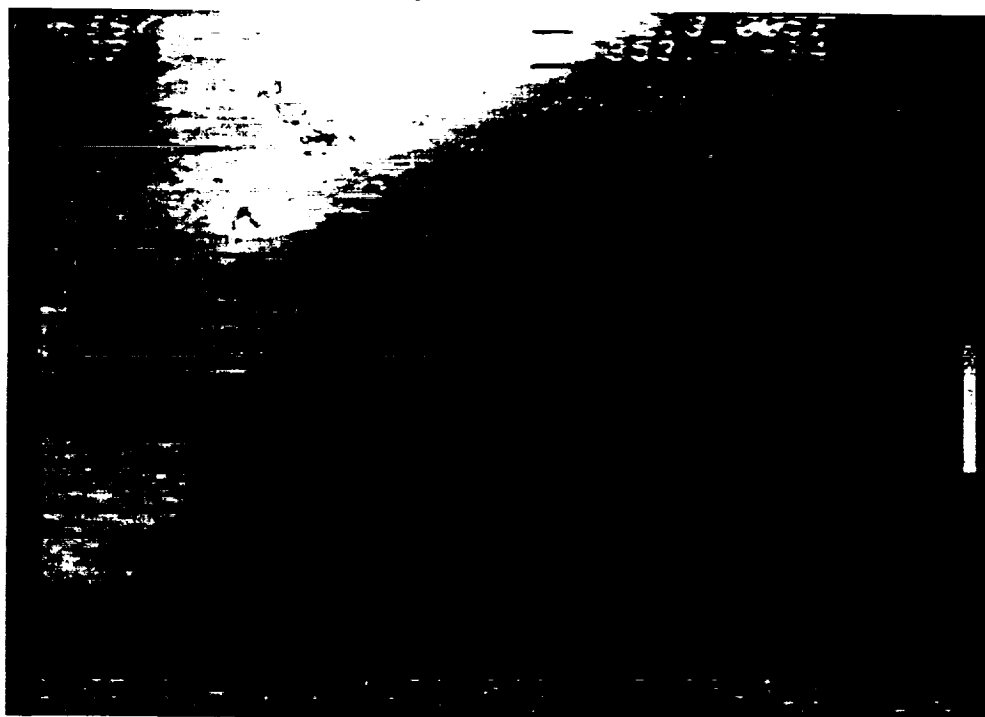


Figure 1b

Fig. 1. (a) Artificial aurora image in 4278 Å. To the left is a quiet auroral arc; in the upper right is the artificial aurora. The image was obtained by the AEPI instrument [11], which viewed downward along the magnetic field direction, during a one-second period beginning at 16:01:59 UT on March 26, 1992. The direction of motion of the Shuttle Orbiter was to the left, so the natural auroral arc is broadened in the horizontal direction by about 10%. The width of the image at the 110-km level is about 80 km. The color bar is linear from top to bottom and extends from 0 to about 5 kR. (b) Same as (a) except that in this case the image was obtained over the one-second period beginning at 15:57:44 UT on March 26, 1992, and the artificial aurora was superimposed upon a large auroral arc.

CRITICAL IONIZATION VELOCITY (CIV) EXPERIMENT

The Critical Ionization Velocity (CIV) theory, first postulated by Alfvén /9/, states that neutral gas travelling perpendicular to a magnetic field will suddenly become ionized when its velocity in the rest frame of the magnetic field reaches a threshold value such that the kinetic energy of the gas in that frame is equal to its ionization potential ($v_{crit} = \sqrt{2e \phi_{ion}/m}$).

The CIV phenomenon has been suspected to play an important role in various plasma dynamics situations ranging from cometary comas and astrophysical problems to spacecraft environment interactions and ionization in magneto-plasma-dynamic (MPD) thrusters. While CIV has been observed in many laboratory experiments, a definitive and unambiguous observation of this phenomenon in space has proved to be elusive. Torbert /10/ gives a review of many of the attempts to observe CIV in the ionosphere. This section reports on a CIV experiment that was performed on the ATLAS 1 mission as part of the Space Experiments with Particle Accelerators (SEPAC) using the plasma contactor (Table 1) in the neutral gas mode.

The SEPAC CIV experiment consisted of a series of 100 ms neutral xenon releases, repeated once every five seconds for five minutes. The release velocity of the xenon from the PC at the 245 psi nominal plenum tank pressure is on the order of 30.5 m/s; therefore, the neutral xenon had essentially the orbital velocity of ≥ 7 km/s when released from the PC regardless of the orientation of the release with respect to the velocity vector. In order to satisfy the CIV criterion, the velocity perpendicular to the magnetic field must exceed the critical value; therefore, the planned experiments were performed at high latitudes, where the angle between the orbital velocity and the field line is nearly 90°.

The CIV experiment was performed twice during ATLAS-1: once in the planned configuration (payload bay in the wake) and once with the payload bay toward the Earth. The latter configuration is not optimum for the CIV experiment because the gas is released perpendicular to the velocity vector, i.e., not into the ram or wake; however, we chose to take advantage of available experiment time with the Orbiter in this attitude.

RESULTS FROM SEPAC DIAGNOSTICS

Figure 2 shows SEPAC diagnostic package (Table 1) data from 16:07:35 to 16:08:05 UT on March 27 (Day 87), 1992. The first CIV experiment began at 16:07:40 UT. The payload bay was toward Earth at that time (Fig. 1b). The top plot shows the neutral gas fast acting valve status as "on" when the valve is open; the valve stays open for approximately 100 msec every 5 sec. The second plot is the Langmuir probe current (top) and voltage (bottom). Before the beginning of the experiment, the probe voltage was swept in order to obtain the ambient electron temperature and density. Once the neutral gas releases began, the voltage was held constant at +9 V (the maximum applied voltage) in order to record density fluctuations. Unfortunately, voltage sweeps immediately before the start of the releases show that the probe does not reach the electron saturation limit at this voltage. During the releases the current does reach the maximum level that can be read by the probe, increasing by a factor of at least 60 as compared to the background level.

COMPARISON WITH CIV MODELS

In the paper by Marshall et al. /11/, a two-part code was used to model possible CIV effects for the experimental configuration of the first CIV experiment. The first part is a linear and quasilinear wave (and instability) model for wave generation, saturation, and particle heating during a CIV interaction given the ambient and release parameters. This model takes into account many realistic effects such as magnetization, full kinetic effects, collisions, spatial effects, and electromagnetic polarization. The second part of the code is a set of necessary conditions or criteria that a CIV release in space must satisfy in order for a CIV interaction to be possible. Most of these criteria have been discussed by Murad and Lai /12/.

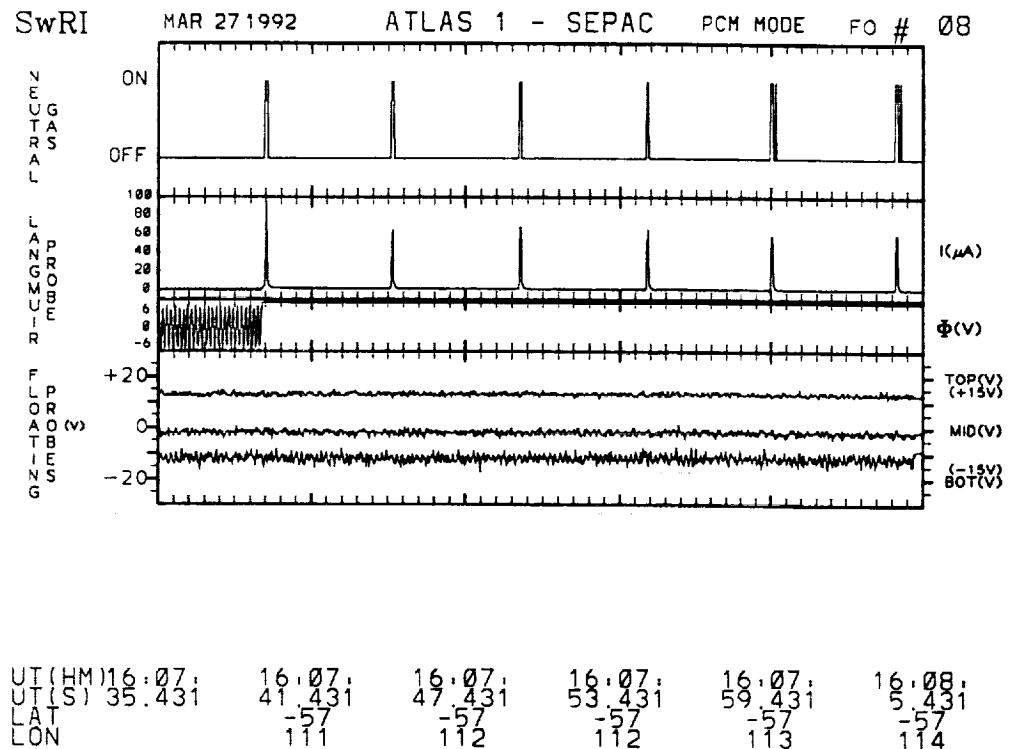


Fig. 2. Data from the SEPAC diagnostic package plotted against universal time from 16:07:35 to 16:08:05 on Day 87 (March 27), 1992. The first panel shows the neutral gas release valve status (ON/OFF). Each pulse lasts 100 msec and represents on the order of 1/6 mole of neutral xenon. The second 2 panels show the Langmuir probe current (top) and applied voltage (bottom). As soon as the releases begin, the probe voltage is held constant at +9 V. The bottom plot shows the voltage on the three sensors of the floating probe. Ancillary data are given at the bottom of the plot along the x axis.

CIV CRITERIA

Marshall et al. /11/ used their model to evaluate several CIV criteria for the SEPAC releases. Their results are summarized in Table 2.

CONCLUSIONS

The prospect for a CIV type interaction for this particular release is good judging from the application of the above criteria. The criteria are mostly (and at worst marginally) met at distances of 100 meters or so from the spacecraft. One criterion not considered stipulates that the dimension of the cloud must exceed the wavelength of the unstable mode responsible for electron energization. The evaluation of this criterion must await the study of the wave physics of this particular release. Finally, criteria for disqualifying the possible role of other ionization mechanisms in these releases (such as charge-exchange and the entrainment of collisionally ionized neutrals to the probe as discussed by Sasaki /20/) have not yet been addressed quantitatively.

TABLE 2 CIV Criteria

Parameter/ Phenomenon	Reference	Criterion	Requirement	Result
Release Velocity	Papadopoulos /13/	$v_{rel} \geq v_{ci}$	$v_{rel} \geq 4.2 \text{ km/s}$	$v_{rel} = 7.4 \text{ km/s}$
Magnetic Field Strength	Axnäs and Brenning /14/	$\omega_{pe}/\omega_{ce} > \sqrt{m_e/m_b}$	$B < .04 \text{ T}$	$B \approx 6 \times 10^{-3} \text{ T}$
Pitch Angle	Lai and Murad /19/	$L\sigma n_b > \sin \alpha > v_{ci}/v_{rel}$ (L = cloud dimension, σ = electron- impact ionization cross-section)	$33 < \alpha < 90$	$\alpha \sim 80^\circ - 90^\circ$
Collisionality	Choueiri et al. /15/	$\Omega_{Hi} > (v_{rel}^2/v_{ci}^2 - 1)^{-1}$	$f_{coll} < 18 \text{ Hz}$	$f_{coll} \geq 96 \text{ Hz}$
Metastable Enhancement	Lai et al. /16,17/	$t_{ion} < \text{lifetime for metastable state}$ ($6s(3/2)_2$)	$t_{ion} < 150 \text{ s}$	$t_{ion} = 3\mu\text{s} - 70 \text{ s}$
Mass Loading	Haerendel /18/ Lai and Murad /19/	$n_b = 0.8 n_a m_a v_A / m_b v_{rel}$	$\Delta n_b = 10^6 \text{ cm}^{-3}$	$\Delta n_b = 10^6 \text{ cm}^{-3}$

Note: v_{rel} is the release velocity perpendicular to the magnetic field (B), v_{ci} is the critical ionization velocity; ω_{pe} and ω_{ce} are the electron plasma and cyclotron frequencies; L is the dimension of the released cloud; σ is the electron-impact ionization cross section; α is the pitch angle; Ω_{Hi} is the Hall parameter for ions; t_{ion} is the ionization time; v_A is the Alfvén velocity; and n_b , m_b , n_a , and m_a are the cloud and ambient densities and masses, respectively.

ACKNOWLEDGEMENTS

Many people have contributed to the SEPAC experiment over the years. Professor Tatsuzo Obayashi, who is recently deceased, was the original principal investigator beginning in 1976. Bill Gibson, Bill Tomlinson, George Ferguson of SwRI and Randy Bounds of Nichols Research contributed extensively to the hardware and software efforts. At ISAS numerous scientists and engineers contributed to SEPAC, including Drs. K. Kuriki, M. Nagatomo, K. Ninomiya, and M. Ejiri. We have benefited greatly from the involvement of co-investigators Dr. Rick Chappell and Professor Peter Banks; the ATLAS-1 crew; the ATLAS Project personnel, under the guidance of Tony O'Neill of MSFC, and Dr. Bob Beattie of Hughes Research Laboratory.

REFERENCES

1. Mende et al., Artificial auroras in the upper atmosphere: 2. imaging results, *Geophys. Res. Lett.*, 495-498, 1993.
2. Obayashi, T., et al., Space experiments with particle accelerators, *Science*, 225, 195-196, 1984.
3. Burch, J. L., et al., Artificial auroras in the upper atmosphere: 1. electron beam injections, *Geophys. Res. Lett.*, 491-494, 1993.
4. Hess, W. N., et al., Artificial auroral experiment: experiment and principal results, *J. Geophys. Res.*, 76, 6067-6081, 1971.
5. Davis, T. N., et al., Artificial aurora experiment: ground-based optical observation, *J. Geophys. Res.*, 76, 6082-6092, 1971.
6. Davis, T. N., et al., Artificial aurora conjugate to a rocket-borne electron accelerator, *J. Geophys. Res.*, 85, 1722-1728, 1980.
7. O'Neil, R. R., E. T. P. Lee, and E. R. Huppi, Auroral O('S) production and loss processes: ground-based measurements of the artificial auroral experiment Precede, *J. Geophys. Res.*, 84, 823-833, 1979.
8. Winckler, J. R., The application of artificial electron beams to magnetospheric research, *Rev. Geophys. Space Phys.*, 18, 659-682, 1980.
9. Alfvén, H. On the Origin of the Solar System, Oxford University Press, Oxford, 1954.

10. Torbert, R. B., Review of critical velocity experiments in the ionosphere, *Adv. Space Res.*, 10(7), 47-58, 1990.
11. Marshall, J. A., et al., CIV experiments on ATLAS 1, *Geophys. Res. Lett.*, 499-502, 1993.
12. Murad, E. and S. T. Lai, personal communication, 1992.
13. Papadopoulos, K., On the shuttle glow: The plasma alternative, *Radio Science*, 19, 571, 1984.
14. Axnäs, I., and N. Brenning, Experiments on the magnetic field and neutral density limits on CIV interaction, *Adv. Space Res.*, 10, 27-30, 1990.
15. Choueiri, E. Y., A. J. Kelly, and R. G. Jahn, The manifestation of Alfvén's hypothesis of critical ionization velocity in the performance of MPD thrusters, *18th International Electric Propulsion Conference*, Alexandria, Virginia, 1985.
16. Lai, S., W. McNeil, and E. Murad, The role of metastable states in critical ionization velocity discharges, *J. Geophys. Res.*, 93, 5871-5878, 1988.
17. Lai, S., E. Murad, and W. McNeil, An overview of atomic and molecular processes in critical velocity ionization, *IEEE Transactions on Plasma Science*, 17, 124, 1989.
18. Haerendel, G., The role of momentum transfer to the ambient plasma in critical ionization velocity experiments, *Technical Report SP-195*, European Space Agency, Neuilly, France, 1983.
19. Lai, S. T., and E. Murad, Inequality conditions for critical velocity ionization space experiments, accepted for publication in *IEEE Transactions on Plasma Science*, 1992.
20. Sasaki, S., et al., An enhancement of plasma density by neutral gas injection observed in SEPAC Spacelab-1 Experiment, *J. Geomag. Geoelect.*, 37, 883-894, 1985.

CIV EXPERIMENTS ON ATLAS-1

J. A. Marshall and J. L. Burch
Southwest Research Institute, San Antonio, Texas

E. Y. Choueiri
Electric Propulsion and Plasma Dynamics Lab, Princeton University, Princeton, New Jersey

N. Kawashima
Institute of Space and Astronautical Sciences, Sagami-hara, Japan

Abstract. A test of the Critical Ionization Velocity (CIV) theory was made with neutral xenon releases from the Space Experiments with Particle Accelerators (SEPAC) hollow cathode plasma contactor onboard the Shuttle Orbiter Atlantis during the ATLAS-1 mission. The gas velocity perpendicular to the Earth's magnetic field was essentially the orbital velocity (7.5 km/s), and thus it exceeded the CIV for xenon. The releases were observed with onboard instrumentation. A factor of 60 enhancement was seen in the Langmuir probe current. Calculations confirmed that release conditions generally satisfied criteria for CIV and predicted a maximum factor of 20 increase in plasma density. Thus, CIV effects were likely to have occurred during the ATLAS-1 experiments.

Introduction

Space Experiments with Particle Accelerators (SEPAC) was the only active experiment in the ATLAS-1 payload, which was carried into a 57°, 290 km orbit by the Shuttle Orbiter Atlantis on March 24, 1992. Although SEPAC was primarily a series of experiments with a 7.6 kW electron beam, in particular aimed at the creation of an artificial aurora, the second SEPAC accelerator, a plasma contactor (PC), was used to perform several tests of the Alfvén Critical Ionization Velocity theory. The CIV theory, first postulated by Alfvén [1954], states that neutral gas travelling perpendicular to a magnetic field will suddenly become ionized when its velocity in the rest frame of the magnetic field reaches a threshold value such that the kinetic energy of the gas in that frame is equal to its ionization potential (ϕ_{ion}): $v_{crit} = (2e\phi_{ion}/M)^{1/2}$.

The CIV phenomenon has been suspected to play an important role in various plasma dynamics situations ranging from cometary comas and astrophysical problems to spacecraft environment interactions and ionization in magnetoplasmadynamic (MPD) thrusters. A recent review of the significance of CIV has been made by Biasca [1992]. While CIV has been observed in many laboratory experiments (see Piel [1990] for a review), a definitive and unambiguous observation of this phenomenon in space has proven elusive. Torbert [1990] reviews attempts to observe CIV in the ionosphere, and Brenning [1992] gives a thorough review of all aspects of CIV.

A CIV study using a xenon gas release from Spacelab was proposed by the AMPS Science Working Group in 1975 (see Möbius [1979]). This method takes advantage of the fact that the Shuttle orbital velocity of >7 km/s exceeds the 4.2 km/s critical ionization velocity for xenon. It has several advantages over sounding rocket experiments,

including better control of the magnetic field configuration, and the possibility of repeating the experiment many times in one mission while varying release parameters. Further, it avoids difficulties with ground based optical observations [Wescott et al., 1992] by using optical diagnostics on the Shuttle, and has a much higher mass flow rate than other satellite experiments, e.g. the APEX xenon releases.

The first Spacelab CIV experiment was performed by ejecting argon plasma at supersonic speeds (near 20 km/s) from a SEPAC plasma accelerator on Spacelab 1. Ionization of the ambient neutrals was reported by Sasaki [1986]. For ATLAS-1, the argon plasma accelerator was replaced by the xenon PC, making it possible to perform the CIV experiment as originally proposed for AMPS.

Hardware

The SEPAC PC is a 25 cm hollow cathode plasma source capable of ejecting 1.6 A of xenon plasma in a continuous mode and/or .15 mole of neutral xenon in 100-ms pulses, and was intended to aid in neutralizing the Orbiter during electron beam firings. In addition to the PC and the electron beam, the SEPAC hardware also included a diagnostics package. Details of the diagnostic instruments are given in Burch et al. [1992]. Figure 1 shows the layout of the SEPAC experiment on the ATLAS-1 pallet. The plasma contactor orifices are approximately 1.5 m from the diagnostics package probes.

The CIV Experiments

The SEPAC CIV experiments, designated Functional Objective 8 (FO8), consisted of a series of 100-ms neutral xenon releases, one every five seconds for five minutes. The release velocity of the xenon from the PC at the 245

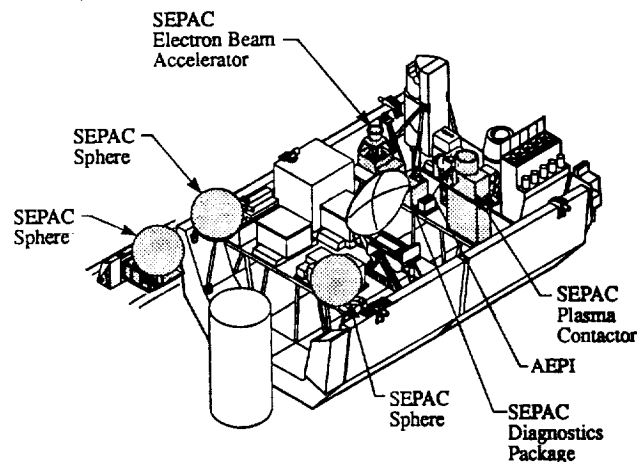


Fig. 1. ATLAS-1 pallet configuration. SEPAC equipment is shaded.

Copyright 1993 by the American Geophysical Union.

Paper number 93GL00593
0094-8534/93/93GL-00593\$03.00

psi nominal plenum tank pressure is only ~ 30.5 m/s, and therefore the neutral xenon will have essentially the orbital velocity of 7.5 km/s when released from the PC regardless of the orientation of the release with respect to the velocity vector. In order to satisfy the CIV criterion, the velocity perpendicular to the magnetic field must exceed the critical value; we therefore planned to perform FO8 at high latitudes, where the angle between the orbital velocity and the field line is nearly 90° .

Figure 2a shows the planned orientation of the Orbiter for the CIV experiment, with xenon released into the wake. FO8 was performed twice during ATLAS-1: once with the payload bay in the wake (Figure 2a) and once with the payload bay toward the Earth (Figure 2b). The latter is not optimum for the CIV experiment because the gas is released perpendicular to the velocity vector, i.e., not into the ram or wake where the plasma environment is more easily modeled; however, we chose to take advantage of available experiment time with the Orbiter in this attitude.

Results from SEPAC Diagnostics

The SEPAC diagnostics package included a Langmuir probe, a floating probe with three vertically spaced sensors, high and low frequency wave receivers and a vacuum gauge. In addition to these diagnostics, the Atmospheric Emissions Photometric Imager (AEPI) was used to obtain images of the neutral gas releases. We plan to report on the optical measurements, as well as the wave data, in a later paper.

Figure 3 shows diagnostics package data from the 16:07:39 to 16:07:40 UT on March 27 (Day 87), 1992, the beginning of the first ATLAS-1 CIV experiment. Universal Time is plotted on the x axis. The payload bay was toward Earth at that time (Figure 2b). All data are plotted with maximum resolution (1 msec, except in the case of the valve status, which is 2 msec). The top plot shows the neutral gas fast acting valve status as "on" when the valve is open; the valve stays open for approximately 100 ms every 5 sec.

The second plot is the Langmuir probe current (top) and voltage (bottom). Before the beginning of the FO, the probe voltage was swept in order to obtain the ambient electron temperature and density. Once the neutral gas releases began, we held the voltage constant at +9 V (the maximum applied voltage) in order to record density fluctuations. Unfortunately, voltage sweeps immediately before the start of the releases show that the probe does not reach the electron saturation limit at this voltage. During the release shown the current does saturate the probe electronics, increasing by a factor of at least 60 as compared to the background level. Although the exact

SEPAC CIV EXPERIMENT (FO 8)

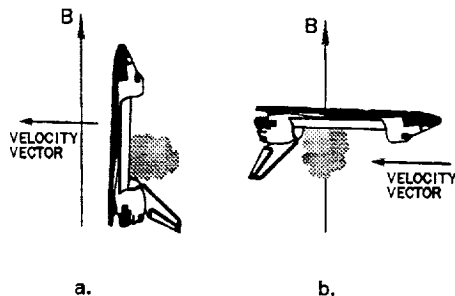


Fig. 2. (a) Orbiter orientation planned for SEPAC CIV experiment and used for FO8-2. (b) Orbiter configuration for FO8-1.

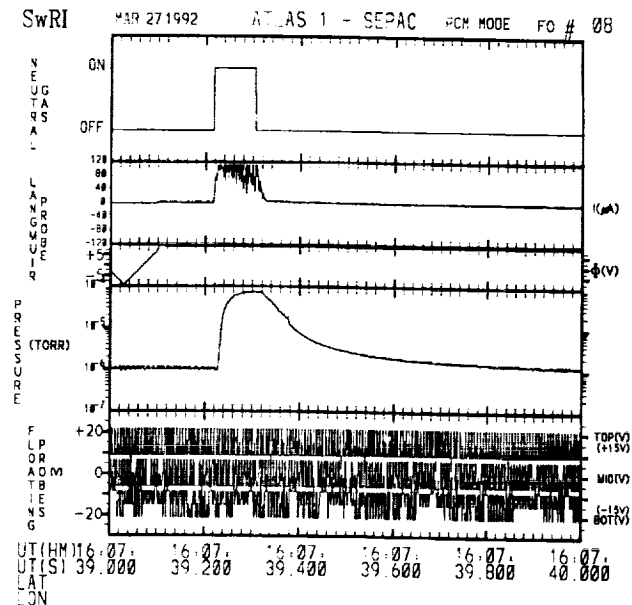


Fig. 3. Data from the SEPAC diagnostics package plotted against universal time from 16:07:39 to 16:07:40 on Day 87 (March 27), 1992.

increase in plasma density cannot be calculated because +9 V does not represent the electron saturation limit, this does indicate a substantial amount.

The third panel shows data from the vacuum ionization gauge, located at the base of the Langmuir probe. The increase in Langmuir probe current shown above precedes the increase in neutral pressure shown here by 14 msec. This lag may occur because the vacuum gauge is farther from the release point than is the Langmuir probe sensor, or it may reflect the response time of the gauge.

The bottom panel shows the voltages on the floating probe top, middle and bottom sensors, each spaced 25 cm apart vertically. The voltages on the top and bottom sensors have been offset by +15 V and -15V, respectively, so that the traces can be distinguished. The data are extremely noisy; however, there is no discernible increase on any sensor during the gas releases, indicating that the Langmuir probe current spikes are due to increases in density and not merely the result of a shift in vehicle potential.

Figure 4 shows a summary plot of the peak Langmuir probe current (solid line) and the peak ambient neutral pressure (dashed line) for each gas release in FO8-1, indicating that the plasma density during neutral xenon pulses is proportional to the amount of xenon released, which declines over the five minute extent of the experiment. Similar data from the second performance of FO8 (FO8-2) show that the level of ionization in that experiment, which was performed with the payload bay in the wake (Figure 2a), was not qualitatively different from that in the first FO8. (Recall that FO8-1 was performed with the payload bay toward the Earth.) Table 1 summarizes the two CIV experiments from ATLAS-1.

Evaluation of CIV Test Criteria

In addition to the relative velocity requirement, there is a set of necessary conditions or criteria that a neutral gas-plasma release in space must satisfy in order for a CIV interaction to be possible. Most of these criteria have been discussed by Lai and Murad [1992]. To compare with the

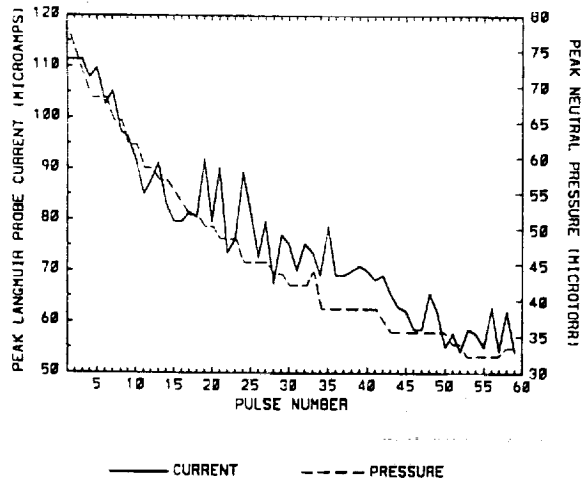


Fig. 4. Summary plot of peak Langmuir probe current (solid line) and peak ambient neutral pressure (dashed line) for each neutral xenon release in the first performance of the SEPAC CIV experiment.

CIV test criteria, we selected a typical 100-ms xenon gas release at 131 g/s from the FO8-1 series. This particular release happened at 16:11:19 UT on Day 87 (March 27) with a spacecraft orbital velocity of 7.5 km/s. The Langmuir probe current-voltage characteristic from immediately before the FO started yielded a density of at least $5 \times 10^4 \text{ cm}^{-3}$, but was too noisy to determine accurately the electron temperature. We selected an electron density of $5 \times 10^4 \text{ cm}^{-3}$ and an electron temperature of 1.1 eV for use in the calculations.

CIV Criteria

CIV-prone Region. Lai and Murad [1992] define a CIV-prone region bounded by distances x_1 and x_2 from the spacecraft. The distance x_1 is the upper bound for the CIV-prone region and is obtained by requiring the ionization time scale to be shorter than the residence time scale of electrons in the spirit of a Townsend criterion for the initiation of a self-sustained discharge. For the above conditions, this distance was calculated to be $x_1 = 134 \text{ m}$ from the spacecraft. At the end of the 100-ms pulse the released gas cloud would have a dimension of 6 m. Since this dimension is smaller than x_1 the release cannot be considered as a steady-state conical beam but rather as a symmetrically expanding cloud.

The distance x_2 is the lower bound for the CIV-prone region and is obtained by requiring the time it takes a magnetic field line to move across the cloud to be shorter than the time needed for the electrons to be heated by the instability fueling the CIV interaction. Assuming that the latter time scale is $30/\omega_{pe}$, as suggested in Tanaka and Papadopoulos [1983], we get $x_2 = 12 \text{ m}$. CIV is therefore

restricted to happen between 12 and 134 m from the release point.

Release Velocity Criteria. Alfvén's original criterion for CIV $v_{rel} \geq v_A$ was satisfied for xenon, whose v_A is only 4.2 km/sec. Another inequality that must be satisfied by the relative velocity, as pointed out by Papadopoulos [1984], states that the v_{rel} must not exceed $(1 + \beta_e)^{1/2} v_A$ (where v_A is the Alfvén velocity and β_e is the electron beta) lest electromagnetic modes decrease the heating efficiency of the instability. This yields an upper limit for v_{rel} of 460 km/sec at x_1 and 400 m/s at x_2 , implying that this criterion is initially violated near the spacecraft where the density is relatively high ($n_e = 1.7 \times 10^{12} \text{ cm}^{-3}$ at x_2 assuming an ionization fraction of 10^{-6}) but quickly becomes satisfied as the cloud recedes from the spacecraft (n_e drops to $2.6 \times 10^4 \text{ cm}^{-3}$ at x_1).

Magnetic Field Strength Criterion. The inequality $\omega_{pe}/\omega_{ce} > (m_e/M)^{1/2}$ was proposed by Brenning and Axnäs [1981, 1990] to set an upper limit on the magnetic field. The smallest value for this upper limit in our particular experiment is calculated to be 0.04 Tesla, which is well above the strength of the local magnetic field, implying that the criterion is satisfied (at both x_1 and x_2).

Pitch Angle Criterion. Lai and Murad [1992], using electron escape arguments, stated that the release pitch angle θ must satisfy the inequality $L \sin \theta > v/v_{rel}$, where L is the dimension of the cloud and σ is the effective cross-section for electron impact ionization of xenon neutrals. This yields $33^\circ < \theta < 90^\circ$ (at both x_1 and x_2) for our case, a condition well satisfied by the release.

Collisionality Criteria. Choueiri et al. [1985] derived from a model of the rate kinetics a condition that must be satisfied by the level of collisionality of the newly produced ions in order for collisions not to disrupt the energization process. This criterion, cast in terms of a condition on the maximum allowable effective Hall parameter for the newly produced ions, Ω_{in} , is $\Omega_{in} > 1/(\bar{v}_{rel}^2/\bar{v}_e^2 - 1)$. This sets an upper limit on the allowable effective collision frequency for the new xenon ions, which is calculated to be about 18 Hz. This criterion is clearly violated at x_2 where the neutral gas density is very high ($n_n = 1.7 \times 10^{12} \text{ cm}^{-3}$) but becomes more tenable toward the outer boundary of the CIV-prone region (the effective collision frequency of the new xenon ions drops to 96 Hz near x_1).

Criterion for Metastable Enhancement. The ionization time from the $(6s[3/2]_2)$ metastable state of xenon is calculated to be 70 s for the conditions at x_1 and 3 μs for the conditions at x_2 . Both values are lower than the metastable lifetime for that state. This implies that the likelihood of sustaining a CIV discharge for this particular release may be enhanced because of ionization from metastable states [Lai et al., 1988; 1989].

Mass Loading. The mass loading effect may reduce the effective relative velocity through strong momentum coupling between the ions produced in the beam and the ionospheric ions [Haerendel, 1983; Lai and Murad, 1992]. This effect sets an upper limit on the plasma density in the beam, n_b , given by Lai and Murad [1992] as $n_b = 0.8n_e M_e \bar{v}_e / M_i \bar{v}_{rel}$. For the conditions of our particular release this translates into a ion density yield of 10^6 cm^{-3} , which is about a factor of 20 increase in the ambient density. The number is of the same order as the factor by which the Langmuir probe current increased during the release.

Prospect for a CIV Interaction. The prospect for a CIV type interaction for this particular release is good judging from the application of the above criteria. The criteria are mostly (and at worst marginally) met at distances close to x_1 from the spacecraft. One criterion not considered stipulates that the dimension of the cloud must exceed the wavelength of the unstable mode responsible for electron

Table 1. Summary of CIV experiments from ATLAS-1

FO	Attitude	Max LP Current (μA)	V_{perp}	Pitch Angle
8-1	Payload bay to Earth	>111.4	7.36 km/s	81°
8-2	Payload bay in wake	>111.4	7.46 km/s	90°

energization. The evaluation of this criterion must await the study of the wave data for this particular release. Finally, criteria for disqualifying the possible role of other ionization mechanisms in these releases (such as charge-exchange and the entrainment of collisionally ionized neutrals to the probe as discussed by Sasaki [1985]) have not yet been addressed quantitatively.

Discussion and Conclusions

Model calculations indicate that the release under study is a good candidate for CIV effects, and predicts a maximum density enhancement in qualitative agreement with the factor of 60 increase seen in the Langmuir probe current. Data taken with the release in the ram compared with data taken from a release perpendicular to the ram show no qualitative difference in the Langmuir probe current. The calculations, however, predict CIV-enhanced ionization to occur between 12 and 134 m from the release point, and it is difficult to determine how the plasma, which should be tied to the magnetic field, could have been transported to the vicinity of the Langmuir probe.

There are possible explanations other than CIV effects for the high probe current. Recalling the probe was not at the electron saturation voltage, it is possible that the density increase may be overestimated compared with the ambient. Alternatively, the density may be due to plasma resulting from collisional interactions between the injected gas molecules and the ambient plasma that is then channeled to the probe by the magnetic field. This effect was observed on Spacelab 1, as described by Sasaki [1985]. The ionization in the two cases studied here does not vary with attitude, however, as was the case in Spacelab 1.

We plan to model releases in other attitudes, hoping to find a case for which the model does not predict substantial CIV density enhancement. Comparison with the current increases in such a case should shed light on the likelihood that the enhancement is due to CIV effects. Optical data, when they are available, will also help to confirm that there was indeed enhanced ionization in the region predicted by our calculations.

Acknowledgements. The authors gratefully acknowledge the work of the entire SEPAC team and the ATLAS-1 POCC Cadre and crew. We also thank Amy Cotton for her painstaking work on the SEPAC data analysis software and Gerry Murphy for a very helpful discussion. This work was supported by NASA contract NAS8-32488 and Air Force contract AFOSR-91-0162.

References

- Alfvén, H., *On the Origin of the Solar System*, Oxford University Press, Oxford, 1954.
- Axnäs, I., and N. Brenning, Experiments on the magnetic field and neutral density limits on CIV interaction, *Adv. Space Res.*, 10, 27-30, 1990.
- Biasca, R., *Numerical Simulation of the Critical Ionization Velocity Mechanism*, PhD thesis, Massachusetts Institute of Technology, Cambridge, MA, 1992.
- Brenning, N., Experiments on the critical ionization velocity interaction in weak magnetic fields, *Plasma Physics*, 23, 967-977, 1981.
- Brenning, N., Review of the CIV phenomenon, *Space Science Reviews*, 59, 209-314, 1992.
- Burch, J. L., et al., Artificial auroras in the upper atmosphere, *Geophys. Res. Lett.*, this issue, 1992.
- Choueiri, E. Y., A. J. Kelly, and R. G. Jahn, The manifestation of Alfvén's hypothesis of critical ionization velocity in the performance of MPD thrusters, *18th International Electric Propulsion Conference*, Alexandria, Virginia, 1985.
- Haerendel, G., The role of momentum transfer to the ambient plasma in critical ionization velocity experiments, Technical Report SP-195, European Space Agency, Neuilly, France, 1983.
- Lai, S. T., and E. Murad, Inequality conditions for critical velocity ionization space experiments, accepted for publication in *IEEE Transactions on Plasma Science*, 1992.
- Lai, S., W. McNeil, and E. Murad, The role of metastable states in critical ionization velocity discharges, *J. Geophys. Res.*, 93, 5871-5878, 1988.
- Lai, S., E. Murad, and W. McNeil, An overview of atomic and molecular processes in critical velocity ionization, *IEEE Transactions on Plasma Science*, 17, 124-134, 1989.
- Möbius, E., R. W. Boswell, A. Piel, and D. Henry, A spacelab experiment on the critical ionization velocity, *Geophys. Res. Lett.*, 6, 29-31, 1979.
- Papadopoulos, K., On the shuttle glow: The plasma alternative, *Radio Science*, 19, 571-577, 1984.
- Piel, A., Review of laboratory experiments on Alfvén's critical ionization velocity, *Adv. Space Res.*, 10(7), 7-16, 1990.
- Sasaki, S., et al., An enhancement of plasma density by neutral gas injection observed in SEPAC Spacelab-1 Experiment, *J. Geomag. Geoelect.*, 37, 883-894, 1985.
- Sasaki, S., et al., Gas ionization induced by a high speed plasma injection in space, *Geophys. Res. Lett.*, 13, 434-437, 1986.
- Tanaka, M., and K. Papadopoulos, Creation of high-energy electron tails by means of the modified two-stream instability, *Physics of Fluids*, 26, 1697-1699, 1983.
- Torbert, R. B., Review of critical velocity experiments in the ionosphere, *Adv. Space Res.*, 10(7), 47-58, 1990.
- Wescott, E. M., H. C. Stenback-Nielsen, and D. L. Hampton, Xenon critical velocity releases from the Activny satellite: Discussion of attempted optical observations, *Geophys. Res. Lett.*, 19, 2079-2081, 1992.
- J. L. Burch and J. A. Marshall, Southwest Research Institute, P.O. Drawer 28510, San Antonio, TX 78228.
- E. Y. Choueiri, Electric Propulsion and Plasma Dynamics Lab, Princeton University, Princeton, NJ 08544.
- N. Kawashima, Institute of Space and Astronautical Sciences, Sagami-hara 229, JAPAN.

(Received 24 August 1992;
revised 19 November 1992;
accepted 7 January 1993.)

Interactions Between the SEPAC Plasma Contactor and the Ionosphere

I. Katz

*S-Cubed Division of Maxwell Laboratories, Inc.*¹

J. N. Barfield,* J. L. Burch,• J. A. Marshall,† and W. C. Gibson^

*Southwest Research Institute*²

T. Neubert

*University of Michigan*³

W. T. Roberts

*NASA/Marshall Space Flight Center*⁴

W. W. L. Taylor

*Nichols Research*⁵

J. R. Beattie

*Hughes Research Laboratories*⁶

Space Experiments with Particle ACcelerator (SEPAC) on Atlas-1 (STS-45) included a plasma contactor to neutralize charge buildup on the orbiter due to electron accelerator operations. The SEPAC plasma contactor operated the same as it had during testing in the laboratory. During SEPAC electron accelerator operations, the contactor emitted currents that helped balance the electron beam current. The

¹ Vice President; Manager, Space Systems Sector, 3398 Carmel Mountain Road, San Diego, CA 92121.

² * Assistant Director, AIAA Member; • Vice President; † Manager, Sensor Design and Calibration; ^ Director, Department of Space Systems, AIAA Member; Division of Instrumentation and Space Research, P.O. Drawer 28510, San Antonio, TX 78284.

³ Associate Research Scientist, Space Physics Research Laboratory, University of Michigan, 2455 Hayward St., Ann Arbor, MI 48109.

⁴ Space Scientist, Payload and Orbital Systems Office, NASA/Marshall Space Flight Center, AL 35812.

⁵ Director of Space Sciences, NASA Programs, AIAA Associate Fellow, 1700 North Moore Street, Suite 1820, Arlington, VA 22209.

⁶ Manager, Plasma Sources Department, AIAA Senior Member, Mail Stop RL-57, 3011 Malibu Canyon Road, Malibu, CA 90265.

Langmuir probe measured the charge exchange ions and the thermal electrons emitted by the contactor. The electric field wave data showed an order of magnitude increase in the 4–8 MHz band. There were no reports of contactor operations interfering with either Orbiter systems or other Atlas-1 experiments.

Nomenclature

A_{probe}	= Langmuir probe area
e	= electron charge
ID	= discharge current
I_i	= ion current generated inside the contactor
IK	= keeper current
I_o	= neutral gas flow
IPC	= current from orbiter chassis to plasma contactor
k	= Boltzman's constant
m_i	= ion mass
MPD	= Magneto Plasma Dynamic
n_o	= neutral gas density
n_{cex}	= charge exchange ion density
n_e	= electron density
n_i	= ion density
P_{cex}	= probability of charge exchange
r	= radial location
r_o	= radius of the plasma contactor orifice
R_{probe}	= distance between the contactor and the probe
sccm	= standard cubic centimeter per minute
STS	= Space Transportation System
T_e	= electron temperature
v_{cex}	= charge exchange ion velocity
VD	= discharge voltage

- v_i = plasma contactor ion velocity
- VK = keeper voltage
- v_o = neutral gas velocity
- $\Delta\phi$ = potential difference from peak plasma potential
- σ = resonant charge exchange cross section

Introduction

Space Experiments with Particle ACceleratorS (SEPAC) on Atlas-1¹ included a plasma contactor to neutralize charge buildup on the orbiter due to electron accelerator operations. During the previous mission (Spacelab 1), at high power levels the SEPAC electron beam returned to the cargo bay causing intense optical emissions.²⁻⁴ The beam returned because the orbiter was unable to collect sufficient electrons from the ionosphere to balance those emitted by the beam. For the reflight on the STS-45 Atlas-1 mission, SEPAC employed three different types of hardware to balance the beam current: three conducting spheres, a neutral gas release system, and a Xenon plasma contactor. This paper focuses on the operation of the plasma contactor, which was used for the first time to neutralize an intense electron beam during a spaceflight. SEPAC hardware included diagnostic instrumentation, which was primarily intended to measure phenomena associated with electron beam interactions with the ionosphere, but also provided useful data about the plasma generated by the plasma contactor, its interaction with the ionosphere, and its ability to control orbiter charging.

Background

Emission of charge neutral plasmas effectively controls spacecraft charging in geosynchronous orbit. Investigations on ATS-6^{5,6} and SCATHA⁷ showed that emission of neutral plasma was more effective in balancing electron currents from the magnetosphere than the emission of electrons alone. Less than a milliampere is needed to control geosynchronous spacecraft charging. In low-Earth orbit, SERT-II (Space Electric Rocket Test II) controlled spacecraft potentials over an 80 volt range by biasing hollow cathode plasma neutralizers.^{8,9} To neutralize the EBA (Electron Beam Accelerator), the first SEPAC flight used an MPD arcjet. The arcjet generated $\sim 10^{19}$ ion-electron pairs during a millisecond pulse that could be repeated every 15 seconds. The resultant plasma dispersed within 100 ms, too short a time to neutralize the orbiter during most of the electron beam operations.²⁻⁴ For the STS-45 mission, instead of the MPD thruster, a plasma contactor was added to SEPAC to provide steady-state charge and current neutralization. Figure 1 shows the configuration of the SEPAC experiment as flown on STS 45. In particular, notice the relative location of the plasma contactor with respect to the diagnostics package.

A plasma contactor is a discharge chamber where an expellant gas (Xenon for SEPAC) is partially ionized by electron bombardment. The resultant dense, low temperature plasma expands into the surrounding space, driven by the quasi-neutral electric fields associated with density gradients. Following earlier work on plasma expansion into vacuum,^{10,11} we assume streaming ions and thermal electrons.^{12,13,14} The electrons that exit the discharge chamber are immediately thermalized, generating turbulence. The ions expand roughly hemispherically from the contactor orifice. The electron population is predominately Maxwellian; that is

the electron density depends exponentially on the potential divided by the electron temperature.

$$\begin{aligned} n_i &= I_i / 2\pi r^2 v_i e \\ n_e &\approx n_i \\ n_e &\approx n_{r=r_0} \exp(e\Delta\phi / kT_e) \end{aligned} \tag{1}$$

Laboratory data shows that the potential of the initial, unexpanded plasma is usually within a few volts of the bombardment chamber anode potential.¹⁵

Contact plasma electrons are two orders of magnitude more mobile than the ions, and normally carry most of the electrical currents. The expanding contact plasma is only weakly collisional and can support electrical currents on the order of the thermal electron current. Only small changes in the potentials from those determined by quasi-neutral plasma expansion are needed to drive significant electron currents.¹²

External to the discharge chamber, the unused neutral expellant interacts strongly with the expanding plasma through resonant charge exchange. Cross sections for resonant charge exchange, σ , approach 100 \AA^2 for Xenon.¹⁶ During charge exchange, slow moving thermal neutral atoms lose an electron to streaming ions. Because of their small velocities, the charge exchange ions respond strongly to density gradient electric fields and expand more nearly isotropically than the forward-streaming contact ions. While only a small fraction of contact ions, the charge exchange ions dominate the plasma density behind the orifice plane.¹⁷ The characteristics of charge exchange plasmas external to an ion thruster have been studied in the laboratory^{17,18} and modeled numerically.¹⁹⁻²¹

The SEPAC Plasma Contactor

The SEPAC plasma contactor²² generates about two amperes of singly charged Xenon ions in a 25 cm diameter discharge chamber. The contactor, built by Hughes Research, is essentially a Kaufman thruster without ion accelerating electrodes. The contactor, as shown schematically in Fig. 2, has separate power supplies for the keeper and main discharge electrodes. The gas is ionized in a two-step process. A small amount, 0.7 sccm (standard cubic centimeter per minute) of Xenon gas, flows through the hollow cathode, through the hole in the keeper electrode and into the main discharge chamber. Typically, the keeper discharge operated at 1.5 amps (IK) and 17 volts (VK). The keeper discharge provides seed ionization and acts as a low impedance cathode which supplies ionizing electrons to the main discharge chamber. Xe gas flows directly into the main discharge chamber at a rate of 36.7 sccm. Small magnets in the discharge chamber enhance the ionization process. When operating at 7 amps (ID), 36 volts (VD) in the main discharge chamber, the plasma contactor ionizes about 75% of the total neutral Xenon gas flow (37.4 sccm) generating 2 A of Xe ions and an equal quantity of electrons. Since the ionization takes place inside the discharge chamber, ambient plasma conditions do not affect the ionization. The dense, $n_e \approx 10^{17} \text{m}^{-3}$, cool, $T_e \approx 2 \text{ eV}$, plasma expands quasi-neutrally into the much less dense, colder surrounding ionosphere.

Because of the large ion current generated by the SEPAC plasma contactor, it could not be determined during the flight whether electrons were indeed the dominant current carriers. The SEPAC contactor was designed to support much larger electron currents than the EBA current; the contactor ion generation rate alone was larger than the maximum EBA current.

The plenum gas pressure, the current and voltages in both power supplies, and the electron current flowing from the contactor to the orbiter chassis were monitored during the flight. Unfortunately, the current from the orbiter to the contactor (IPC) was monitored only when it was positive, so no information about plasma contactor electron emission was obtained.

The SEPAC plasma diagnostics package included a cylindrical Langmuir probe located, as indicated in Fig. 3, 1.37 m toward the center of the orbiter cargo bay and 0.6 m below the contactor orifice. The 4 mm diameter, 20 cm long probe was swept ± 9 V. As was seen in the first flight, the probe positive sweep voltage was not enough to observe electron current saturation due to the orbiter negative floating potential.

The SEPAC plasma instruments were located to the side and behind the contactor orifice and, consequently, measured primarily properties of the secondary, charge exchange plasma, as opposed to plasma ions generated inside the discharge chamber.

Flight Results

Atlas-1 was launched on March 24, 1992 aboard the orbiter Atlantis mission STS-45 in a 300 km altitude, 57° inclination orbit. During the week long mission, SEPAC performed 27 separate experiments using the plasma contactor, covering most orientations with respect to the earth's magnetic field and orbiter velocity vectors, during both day and night, and near the Jicamarca radar observatory. For each of the 27 experiments, the contactor was restarted and operated flawlessly for a total of 7.3 hours, until the supply of Xenon gas was depleted. The plasma contactor electrical data was the same as observed during laboratory testing. Consistently stable voltages

and currents were seen in both the keeper and discharge circuits throughout the flight. All cathode starts occurred within a second of keeper voltage turn on; no high impedance modes were observed. Postflight examination confirmed the telemetry; all contactor circuits were nominal and the Xenon tank was empty. Most of the gas had been expended during SEPAC neutral gas release experiments. The plasma cloud was observed from Jicamarca. In the observation of the near cloud, it had a scattering cross section of about 20 dB larger than that of the orbiter.²³

Langmuir Probe

Compared with the ambient ionosphere, during contactor operation the Langmuir probe showed a hotter, order-of-magnitude denser plasma. As can be seen in Fig. 4, the Langmuir probe traces were noisy both with the contactor on and off. These measurements were made when the beam was off and the orbiter was in the earth's shadow. Figure 4 shows probe currents when the contactor was in the wake of the shuttle and when the contactor was in the ram. While electron current saturation was not observed, enough of the electron trace is available to fit a temperature. The ion current collected is determined from a least squares fit of points with negative voltages; the electron temperature was determined from a fit to the points from 1.80 V to 5.96 V for the wake case, from 3.8 V to 8 V for the ram case, and from 7.9 V to 9.5 V for the ram case with the contactor off. For the cases examined, the electron current fit an exponential fairly well, with an electron temperature between 1.5 and 2.1 eV. As Table 1 shows, the highest temperatures occurred when the contactor was in the wake. Closer interaction with the cooler ionosphere may lower the contactor plasma electron temperature.

Because the Langmuir probe was behind the main contactor orifice, it presumably measured the secondary ions generated by charge exchange occurring in front of the orifice between the main plume and un-ionized Xenon. We can test this hypothesis by comparing the measured ion currents with ion currents expected from charge exchange.

Assuming the neutral Xenon emanating from the orifice expands into a π solid angle,

$$n_0(r) = \frac{I_0}{e \pi r^2 v_0} \quad (2)$$

As long as the neutral gas is not depleted, the probability of charge exchange, P_{cex} , external to the contactor is

$$P_{\text{cex}} = \int_{r_0}^{\infty} n_0(r) \sigma dr \approx \frac{I_0 \sigma}{e \pi r_0 v_0} \quad (3)$$

The median distance from the orifice for charge exchange is $2r_0$. Assuming that the charge exchange ion expansion is spherical, and noting that the distance to the probe is large compared with the orifice size, we can estimate the current to the Langmuir probe,

$$I_{\text{probe}} = \frac{A_{\text{probe}}}{4\pi R_{\text{probe}}^2} P_{\text{cex}} I_i \quad (4)$$

The probe area used is the cross section to streaming flow, $8 \times 10^{-4} \text{ m}^2$. Taking the neutral gas velocity to be 300 m/s, the probability of charge exchange ranges from 7% if the contactor ionizes 50% of the Xenon, down to 3% if the contactor ionizes 80% of the Xenon. During laboratory operation, this was the range of expellant utilization observed. With the flight parameters expellant utilization in the lab was 75%. The predicted range of probe currents due to charge exchange is 1.7 μA to 2.7 μA . The

observed saturation ion currents extrapolated to zero potential range between 1.9 μA and 3.1 μA , consistent with this simple picture.

The charge exchange ion density, n_{cex} , is approximately

$$n_{\text{cex}} \approx \frac{P_{\text{cex}} I_i}{e 4\pi r^2 v_{\text{cex}}} \quad (5)$$

Because the shuttle floats negative, the potential difference between the discharge chamber anode and the local environment is less than the 36 V discharge potential. This potential provides an upper bound on the charge exchange ion velocity, 7300 m/sec. For a charge exchange current of 2 μA , the charge exchange plasma density at the probe would be at least $2 \times 10^{12} \text{ m}^{-3}$. This density is also consistent with the Langmuir probe not showing electron saturation. The corresponding electron saturation current is about 200 μA , far in excess of 112 μA , the maximum current that the probe was capable of measuring. The voltage sweep also limited the probe's operation. From the analyzed data it appears that the saturation current would occur at about 10 V positive, which is above the upper end of the probe voltage sweep range.

Charge Control during EBA Operations

During joint EBA and plasma contactor operations, the contactor current neutralized a portion of the EBA electron current. Data shows that for an EBA emission current greater than 100 mA, current flowed between the contactor and the orbiter chassis. Figure 5 shows an example in which the EBA current reached 0.8 A. These measurements were made in the earth's shadow with the bay facing up. The figure shows the electron beam voltage (top) in volts, the electron beam current (middle) in amperes, and the current from the orbiter chassis to the plasma

contactor (bottom) in amperes. The variation in the beam was preprogrammed. In this case the plasma contactor accounted for more than half the return current. The contactor current was consistently less than the EBA current. This is consistent with preflight expectations that the orbiter exposed conducting surface would collect thermal electron current and the contactor would make up the difference in order to keep the orbiter from charging. Since the orbiter did not charge, the beam escaped even at the highest currents. During the flight, the electron beam generated artificial aurora in the upper atmosphere more than a hundred kilometers from the orbiter.¹

At maximum EBA electron current, 850 mA, the plasma contactor emitted 650 mA. Because the contactor generated 2 A of ions, it is unclear from the data whether the contactor current was carried by electrons flowing in from the ionosphere or by ions flowing from the contactor out to the ionosphere. The ambient environment had no effect on plasma contactor operation, since the plasma produced by the contactor overwhelmed the background plasma in the vicinity of the shuttle. Contrary to some expectations, there were no observations of any visible beam plasma discharges during plasma contactor operations.

Every time the contactor discharge was started, a current spike of the order of 100 mA of current was emitted for a few tenths of a second. Figure 6 shows the plasma contactor emitting current after turn on, with neither neutral gas nor EBA emission. These measurements were made in the earth's shadow with the bay facing down. The bottom two curves are the Langmuir probe potential in volts and current in microamperes. The middle curve is the current from the orbiter chassis to the plasma contactor in amperes. The top two curves are from the wave detectors. The figure shows a current spike of 70 mA at contactor turn on. While probably

associated with differential charging of nearby orbiter surfaces, no quantitative model of this unanticipated emission has been developed.

The contactor currents during SEPAC neutral gas release experiments are not understood. During EBA operation, the neutral gas release occurred just prior to the electron beam turn on. Figure 7 shows typical behavior of the plasma contactor current during a neutral gas release. These measurements were made in the earth's shadow with the bay facing up. The bottom curve shows the neutral gas release. The next curve shows the current from the orbiter chassis to the contactor in amperes. The top two curves are the electron beam potential in volts and current in amperes. Note that the potential variation is shown on an expanded scale. The plasma contactor current shows an ampere level surge during the gas release, followed by a rapid decay until beam turn on. The source of these electrons and the current closure path are not presently known. When the electron beam is turned on, the contactor current slowly rises to a value greater than without neutral gas, and then decays slowly.

Field Fluctuations

The diagnostics package included a wave receiver connected to a half meter electric field antenna. Both narrow band and broad band signals were measured. The broad band receiver measured the gain necessary to output a 1 V signal in three frequency ranges. The antennas were located adjacent to the Langmuir probe. The AGC (Automatic Gain Control) High signal is for the 4–8 MHz band. The AGC Low signal is for the 400 Hz–10 KHz band and comes from a Faraday cup mounted atop the high frequency antenna. The operation of the plasma contactor had the greatest effect in the 4–8 MHz band, the highest frequency measured. Increases of greater

than 20 dB were observed in the electric field energy compared with the ambient plasma. During some contactor operations, when the cargo bay was in the ram, the wave intensity was sufficient to saturate the receiver, corresponding to fluctuating fields of approximately 1 V/m. When the cargo bay was not in the ram, the intensity of the fluctuating fields was lower, the order of a tenth of a volt per meter. Figure 6 shows electric field wave data measured during SEPAC plasma contactor operation. The top two curves are the AGC Low and AGC High data. The data shown indicates oscillating electric fields of order 0.1 V/m. During this period the Langmuir probe was held at a constant potential in order to measure the density fluctuations. The noisy current reflects the variation in the density. The plasma contactor electromagnetic radiation did not interfere with orbiter systems.

Intense electrostatic fluctuations in the contactor plasma are consistent with the Langmuir probe current fluctuations observed when the probe bias voltage was fixed. Published models of hollow cathode plasma contactors predict large amplitude electrostatic turbulence as a result of electrons streaming from the cathode into the contactor plasma.^{12,24} The cathode electrons are accelerated by the discharge potential and form an unstable beam in the local dense plasma. These streaming electrons ionize the contactor gas, generating the contactor plasma. The beam also generates intense electrostatic waves which scatter and thermalize part of the beam. Not presently understood is how the electrostatic turbulence decays.

Summary

During the Atlas-1 mission (STS-45), the SEPAC plasma contactor operated the same as it had during testing in the laboratory. While there were no measurements in the contactor plume, the charge exchange plasma behind the contactor dominated

Langmuir probe currents and was consistent with previous, ground-based measurements. During SEPAC electron accelerator operations the contactor emitted currents that helped balance the electron beam current. There was no evidence of charging, electron beam return, or beam plasma interactions during plasma contactor operations. Highest electron temperatures were observed during deep wake operations, suggesting that thermal conduction with the ionosphere tended to cool the expanding contactor plasma. During plasma contactor operations the electric field wave data showed an order of magnitude increase in the 4–8 MHz band. There were no reports of contactor operations interfering with either Orbiter systems or other Atlas-1 experiments.

Acknowledgments

The authors gratefully acknowledge the work of the entire SEPAC team and the Atlas-1 POCC cadre and crew. This work was supported by NASA Contracts NAS8-32488 and NAS8-35350. Dr. Ira Katz would like to thank the Space Station Freedom Program for enabling his participation in SEPAC and Dr. V. A. Davis for help in preparation of this paper.

References

¹ Burch, J. L., Mende, S. B., Kawashima, N., Roberts, W. T., Taylor, W. W. L., Neubert, T., Gibson, W. C., Marshall, J. A., and Swenson, G. R., "Artificial Auroras in the Upper Atmosphere 1. Electron Beam Injections," *Geophysical Research Letters*, Vol. 20, No. 6, 1993, pp. 491-494.

² Sasaki, S., *J. Spacecraft*, 23, 2, pp. 194, 1986.

- ³ Obayashi et al., *Science*, 225, 195, 1984.
- ⁴ Sasaki, S., et al., *Geophys. Res. Lett.*, 12, 10, 1985, pp. 647-650.
- ⁵ Olsen, R. C., "Experiments in Charge Control at Geosynchronous Orbit - ATS-5 and ATS-6," *J. Spacecraft*, 22, 1985, pp. 254-264.
- ⁶ Purvis, C. K., Bartlett, R. O. and DeForest, S. E., "Active Control of Spacecraft Charging on ATS-5 and ATS-6," in *Proceedings of the Spacecraft Charging Technology Conference*, C. P. Pike, R. R. Lovell, Eds., 1977, pp. 107-120.
- ⁷ Cohen, H. A., Adamo, R. C., Aggson, T., Chesley, A. L., Clark, D. M., Damron, S. A., Delorey, D. E., Fennell, J. F., Gussenhoven, M. S., Hanser, F. A., Hall, D., Hardy, D. A., Huber, W. B., Katz, I., Koons, H. C., Lai, S. T., Ledley, B., Mizera, P. F., Mullen, E. G., Nanevich, J. E., Olsen, R. C., Rubin, A. G., Schnuelle, G. W., Saflekos, N. A., Tautz, M. F. and Whipple, E. C., "P78-2 Satellite and Payload Responses to Electron Beam Operations on March, 30, 1979," in *Spacecraft Charging Technology*, 1980, NASA CP 2182, AFGL-TR-81-0270, pp. 509-559, 1981.
- ⁸ Kerslake, W. and Domitz, S., "Neutralization Tests on the SERT II Spacecraft," AIAA Paper 79-2064, 1979.
- ⁹ Jones, S. G., Staskus, J. V. and Byers, D. C., "Preliminary Results of SERT II Spacecraft Potential Measurements Using Hot Wire Emissive Probes," AIAA Paper 70-1127, 1970 (see also NASA TM X-2083, 1970).
- ¹⁰ Crow, J. E., Auer, P. J. and Allen, J. E., *J. Plasma Phys.*, 14, 65, 1975.

- 11 Gurevich, A. V., Pitaevskii, L. P., and Smirnova, V. V., "Ionospheric Aerodynamics," *Space Sci. Rev.*, 9, 805, 1969.
- 12 Davis, V. A., Katz, I., Mandell, M. J. and Parks, D. E., "Hollow Cathodes as Electron Emitting Plasma Contactors: Theory and Computer Modeling," *J. Spacecraft*, 25, 2, 1988, pp. 175-179.
- 13 Parks, D. E., Katz, I., Buchholtz, B., and Wilbur, P., "Expansion and Electron Emission Characteristics of a Hollow Plasma Contactor," submitted for publication to *Journal of Applied Physics*, April, 1993.
- 14 Williams, J. D., and Wilbur, P. J., "Electron Emission from a Hollow Cathode-Based Plasma Contactor," *Journal of Spacecraft and Rockets*, Vol. 29, No. 6, 1992, pp. 820-829.
- 15 Hayakawa Y., Miyazaki, K., and Kitamura, S., "Measurements of Electron Energy Distributions in a 14 cm Diameter Ring Cusp Ion Thruster," AIAA Paper 89-2715.
- 16 Rapp, D. and Francis, W. E., "Charge Exchange between Gaseous Ions and Atoms," *J. Chem. Phys.*, 37, 11, 1961, pp. 2631.
- 17 Kaufman, H. R., "Charge-Exchange Plasma Generated by an Ion Thruster," NASA CR-135318, 1977.
- 18 Carruth, M. R. and Brady, M. E., "Propagation of Charge-Exchange Plasma Produced by an Ion Thruster," AIAA Paper 80-1388, 1980.

- 19 Katz, I., Parks, D. E., Mandell, M. J., and Schnuelle, G. W., "Parasitic Current Losses Due to Solar-Electric Propulsion Generated Plasma," *J. Spacecraft*, 19, 2, 1981, pp. 129-132.
- 20 Carruth, M. R., Jr., and Pawlik, E. V., "Interactions Between a Spacecraft and an Ion Thruster Produced Environment," AIAA paper 79-2107, 1979.
- 21 Staggs, J. F., Gula, W. P., and Kerslake, W. R., "Distribution of Neutral Atoms and Charge-Exchange Ions Downstream of an Ion Thruster," *Journal of Spacecraft and Rockets*, Vol. 5, No. 2, 1968, pp. 159-164.
- 22 Beattie, J. R., Marshall, J. A., Burch, J. L., and Gibson, W. C., "Design, Qualification, and On-Orbit Performance of the ATLAS Plasma Contactor," to be presented at the 1993 Electric Propulsion Conference, AIAA Paper.
- 23 Jost, R.J., Neubert, T., Farley, D. T., Rodriguez, R., Calderon, C., Woodman, R., and Burch, J. L., "Radar observations of ATLAS-1 plasma contactor disturbances from Jicamarca observatory," *EOS*, Vol. 73, No. 43, Supplement, 1992, p. 412.
- 24 Hastings, D. E., "Enhanced Current Flow Through a Plasma Cloud by Induction of Plasma Turbulence, *Journal of Geophysical Research*, Vol. 92, No. A7, 1987, pp. 7716-7722.

Figure Captions

- Figure 1. Configuration of the SEPAC experiment as flown on STS 45.
- Figure 2. Schematic of the SEPAC plasma contactor.
- Figure 3. Relative placement of the plasma contactor and the Langmuir probe in the shuttle orbiter cargo bay.
- Figure 4. Langmuir probe currents.
- Figure 5. Flight data showing current collected by the plasma contactor during SEPAC Electron Beam Accelerator (EBA) operation.
- Figure 6. Plasma contactor emitting current after turn on, with neither neutral gas nor EBA emission. Also shown is electric field wave data measured during SEPAC plasma contactor operation.
- Figure 7. Plasma contactor current during neutral gas release.

Table 1.
Electron Temperatures and Ion Currents during Plasma Contactor Operation

Time (GMT)	Orientation	T_e (eV)	Ion Current (μ A)
87/01:15:18	ram	1.5	2.1
88/01:14:10	wake	2.1	0.6
89/11:51:46	down	1.9	2.2
90/18:50:5	down	1.2	3.1

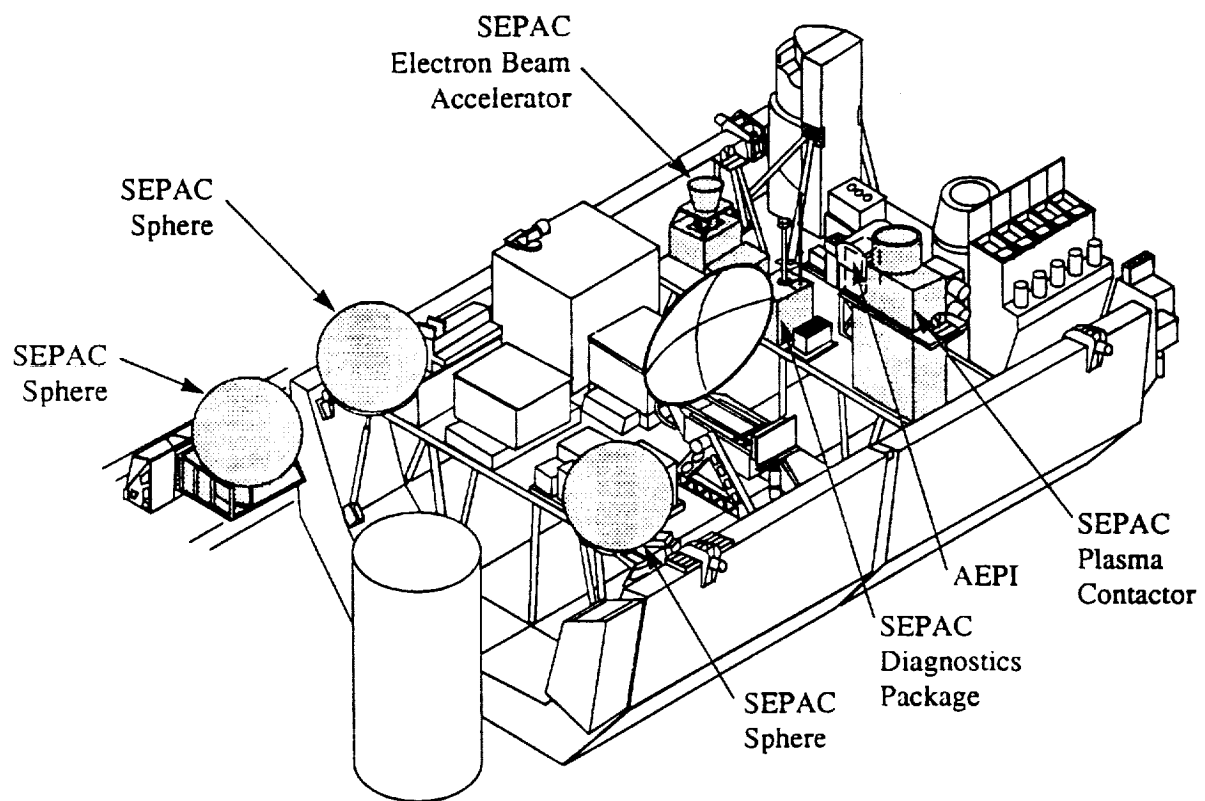


Figure 1.

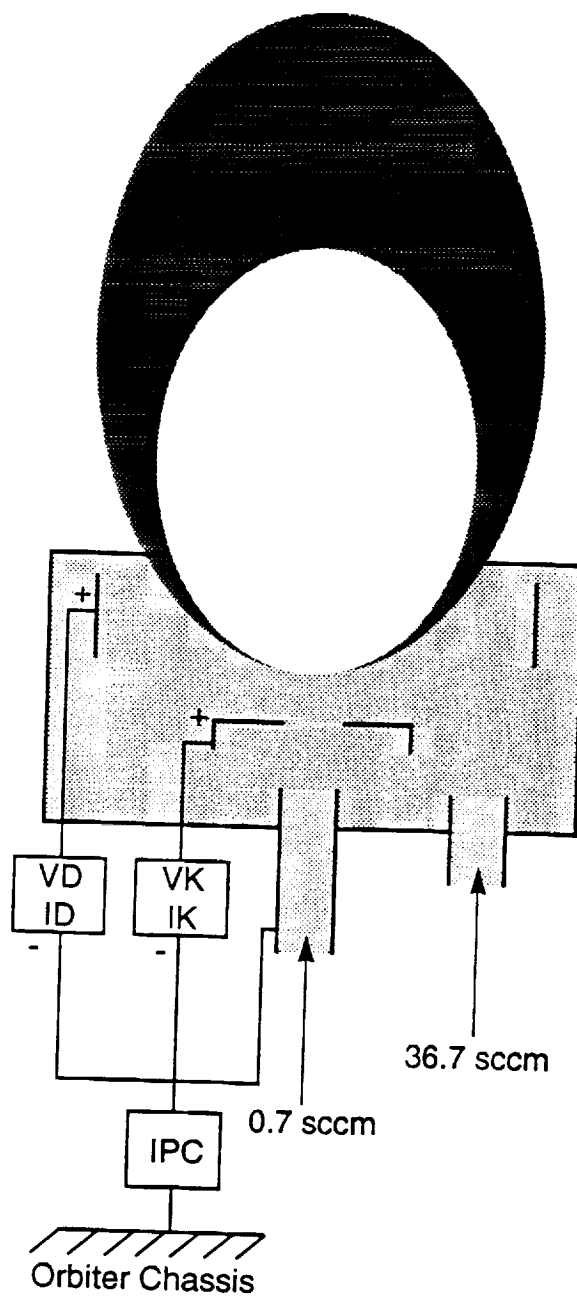


Figure 2.

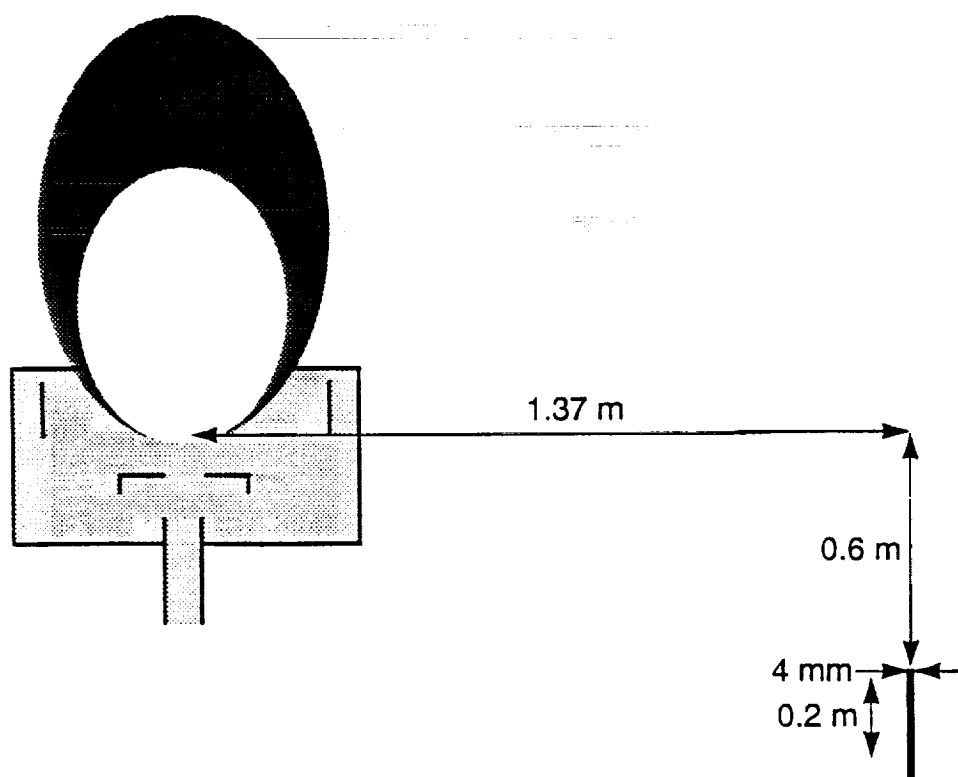


Figure 3.

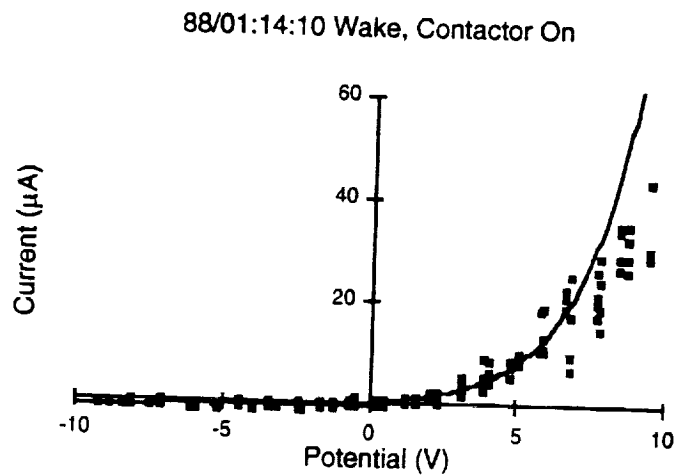
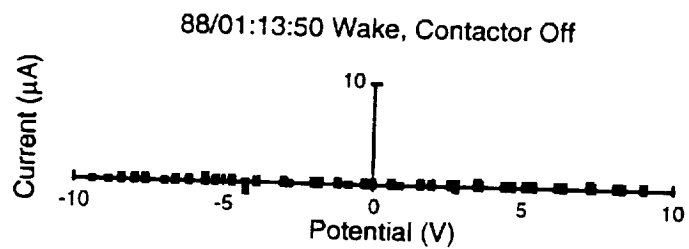
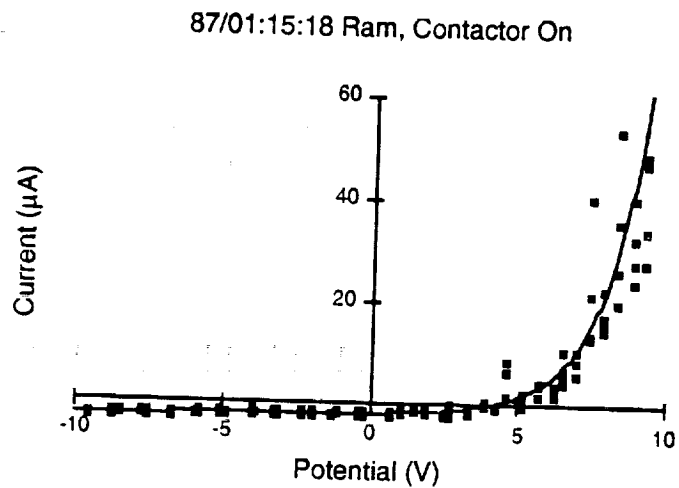
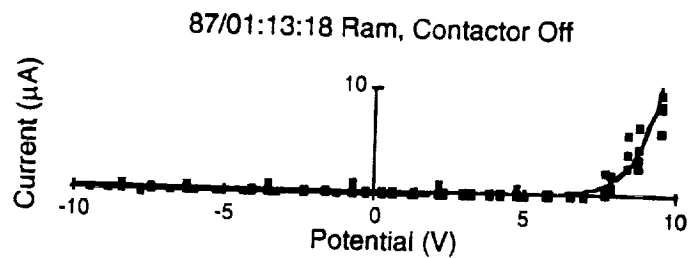


Figure 4.

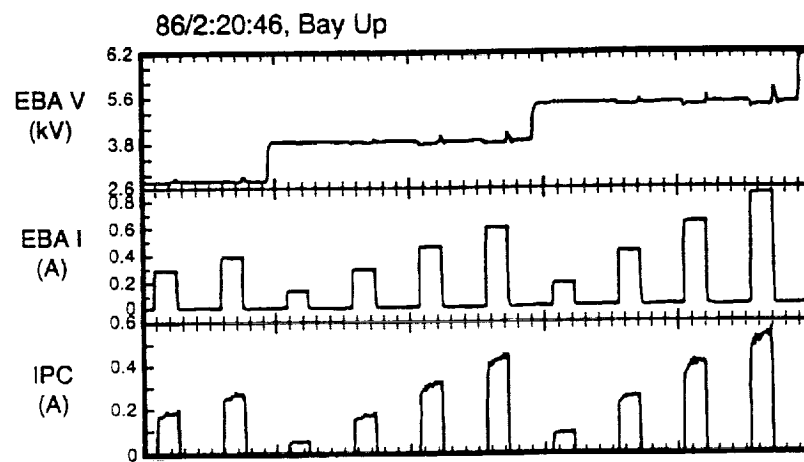


Figure 5.

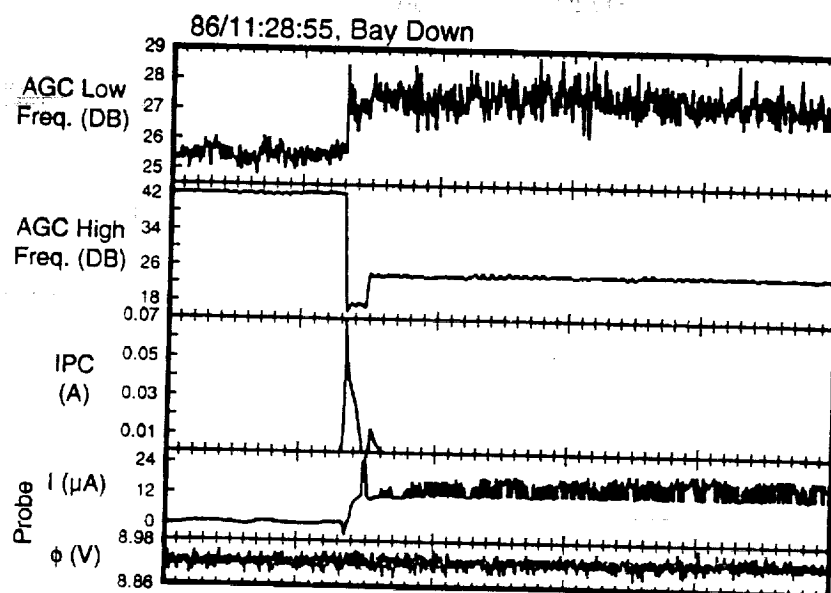


Figure 6.

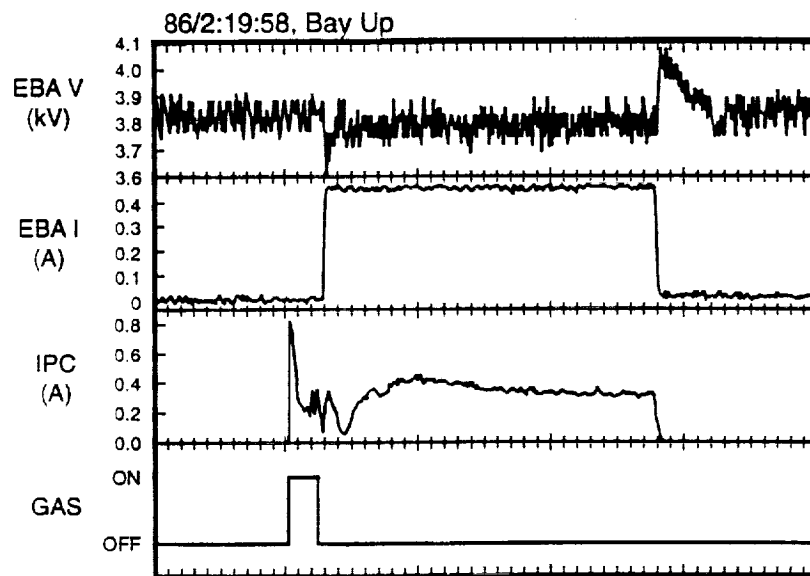


Figure 7.